Role of water in radiochromic LiPCDA monomer crystal packing and radiotherapy dose response

ROHITH KAIYUM

A THESIS SUBMITTED TO

THE FACULTY OF GRADUATE STUDIES

IN PARTIAL FULFILLMENT OF THE REQUIREMENTS

FOR THE DEGREE OF

MASTER OF SCIENCE

GRADUATE PROGRAM IN PHYSICS AND ASTRONOMY

YORK UNIVERSITY

TORONTO, ONTARIO

APRIL 2021

ABSTRACT

Radiochromic films comprised of lithium-10,12-pentacosa diynoate (LiPCDA) crystals, a form of diacetylene, have been developed for *in vivo* real-time dosimetry. The polymerization of LiPCDA results in a change in optical density that is related to the absorbed dose. The dose response of diacetylene monomers is dependent on their packing, determined by the R groups. LiPCDA used in commercial film can have two distinct dose sensitive forms, 635LiPCDA and 674LiPCDA, with peak absorbances occurring at 635 nm and 674 nm, respectively. While the two forms do not differ in their R groups, they have different dosimetric behaviours. The 674LiPCDA achieved through desiccation of 635LiPCDA was 3-fold less sensitive to dose and had ~7-fold higher dynamic range. This indicates that the dosimetric behaviour of radiochromic crystals is primarily dependent on structure, controlled by more than just the chemical composition of individual monomers as water appears to have a role in the packing.

Acknowledgments

I have so many wonderful, dedicated mentors to thank. Thank you for your support, for opening the door for me to share my work at various conferences, for giving me exciting research ideas, developing my academic skillset, and for all of the many opportunities that you provided me. Over the past years, I have learned a lot from an amazing team of researchers and collaborators. Thanks to my team, I now have many experiences under my belt that are rare for a graduate student to have such as building a new lab.

I would like to thank my two supervisors Professor Ozzy Mermut and Dr. Alexandra Rink for being there when I needed support with paper edits, experiment design and training. Thanks also for believing in me as a graduate student and indulging in my many for fun experiments. Many thanks to Dr. Chris Schruder for suggestions and feedback on my experimental designs and useful discussions.

I thank my family for all of their encouragement, support, and love over the past years. I thank my mom for never doubting the decisions I made and always encouraging me to reach my goals. I thank my fiancée Kaitlin McNeil for her love and support in everything I do, for making sure I can tackle my every day and for being there with me every step of the way.

Thank you to everyone for your contributions to my project and for helping me to put together a body of work that I am passionate about and very proud of.

Table of contents

List of figures

List of tables

List of abbreviations and symbols

ΔA	Change in absorbance
ΔOD_{net}	Change in net optical density
635LiPCDA	LiPCDA with absorbance peak maximum at 635 nm
674LiPCDA	LiPCDA with absorbance peak maximum at 674 nm
cGy	centiGray
D	Dose
DesEBT-3	Desiccated EBT-3 film
DNA	Deoxyribonucleic acid
EBT	Commercial radiochromic film for external beam therapy
EBT-3	3rd generation of EBT film
Gy	Gray unit of dose (J/kg)
IR	Infrared
LINAC	Linear accelerator
LiPCDA	Lithium pentacosa-10,12-diynoate
MD-55	Commercial radiochromic film using PCDA active component
OD	Optical density
PCDA	Pentacosa-10,12-diynoic acid
QA	Quality assurance
R	A hydrogen or hydrocarbon side chain group attached to a molecule
UV	Ultraviolet
Z_{eff}	Effective atomic number
λ_{max}	Wavelength of maximum absorbance

Chapter 1: Introduction and hypothesis

1.1 Radiotherapy and dosimetry

It was estimated by the Canadian Cancer Society that there would be 225,800 new cancer patients in 2020[1] with approximately 50% of patients receiving radiation therapy during the course of illness[2]. During a radiotherapy procedure, ionizing radiation is administered either internally (known as brachytherapy) by implanting a radioactive isotope emitting gamma or beta rays, or externally (known as external beam) with high energy X-rays or electron beams delivered with a clinical linear accelerator (LINAC). High energy photons (X-rays or γ-rays) are used to indirectly ionize deoxyribonucleic acid (DNA), disrupting the genes of cancerous cells, which either destroys the cell or prevents cellular mitosis[3–5]. Irradiated healthy tissue may also be damaged as exposure of healthy tissue to radiation is unavoidable[6]. For this reason, radiation is delivered in segments, known as *fractions*, over a few days[7] or weeks[4] to allow for partial repair of normal cells.

The absorbed energy per unit mass of material due to ionizing radiation exposure is referred to as *dose*, measured in units of Gy (Gy = 1 J/kg)[8]. Dosimetry is the measurement and analysis of absorbed dose by a living organism or substance. A typical radiotherapy prescription in external beam is characterized by the total dose to the tumour. However, dose distribution, and not just prescribed dose, is important for tumour control and limiting radiation related side effects. Prior to treatment, a radiotherapy treatment plan with three-dimensional dose distribution is developed. To ensure patients safely receive their prescribed dose, pre-treatment quality assurance (QA) dosimetric tests[9,10] are performed on tissue mimicking phantoms that have a similar dose response to water. These phantoms are irradiated and the dose response is measured against the expected dose to ensure that the treatment is deliverable according to the plan criteria[11]. Pre-treatment QA is the current standard procedure for most radiotherapy clinics, but it does not provide information on the actual dose delivered to the patient[12,13].

Recent treatment techniques have been impacted by advances in radiotherapy technologies. Strategies have shifted towards plans that deliver higher doses of radiation with lower fractions. High dose plans are made possible with technologies such as volumetric modulated arc therapy[14] and intensity-modulated radiation therapy[15,16] as well as image guidance[16]. This is because they allow for tighter margins around the target and conformal dose distribution to the target volume[18,19] while reducing the dose to surrounding organs at risk (Figure 1).

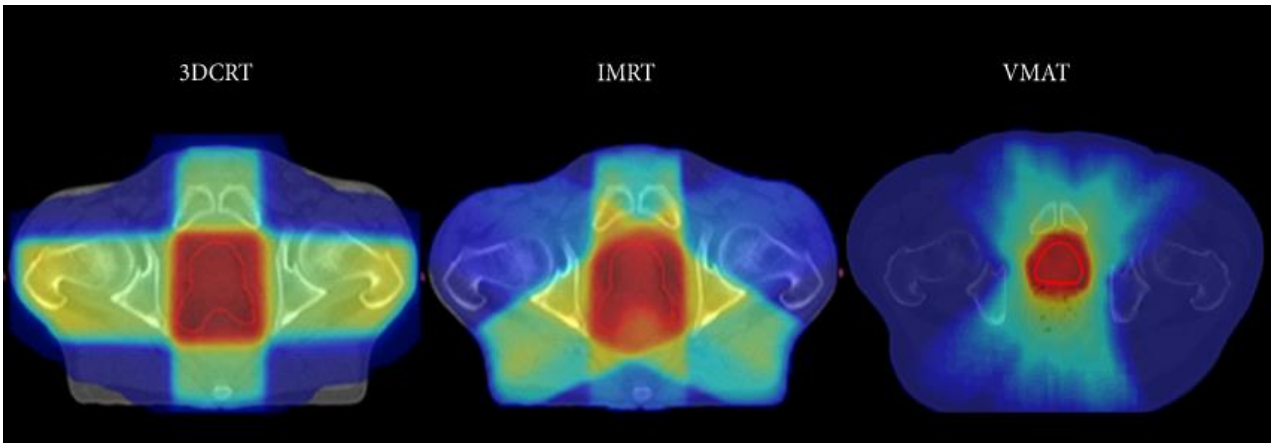

Figure 1: Examples of dose distribution using 3DCRT: 3-dimensional conformal radiotherapy, IMRT: intensity modulated radiotherapy and VMAT: volumetric modulated arc therapy. The red area represents the high dose region and the dark blue surface the low dose region. Vanneste *et.al*[20]

However, the complexity and number of moving components involved in these treatments leave them vulnerable to many sources of error compounded on top of setup errors, changes in anatomy, patient motion, or motion of the inner organs[21]. Many of these factors have been studied independently, but the errors are able to combine to a larger effect on treatment not observed during independent measures. Therefore, it was recommended by the International Atomic Energy Agency to perform *in vivo* dosimetry for all groups of patients undergoing radiotherapy[22]. Thus, for a true measure of actual dose delivered to a patient, real-time *in vivo* dosimetry is needed.

1.2 *In vivo* dosimetry

In radiation therapy, *in vivo* dosimetry is the measurement of radiation dose absorbed by the patient during treatment. This can be done by temporarily placing a dosimeter into the patient through a catheter or an orifice, or by placing it on the skin[23]. *In vivo* dosimetry provides an independent verification of the treatment procedure to identify errors in dose distribution calculations, machine calibration and patient setup[23,24]. Thus, it is recommended by several national and international agencies[22,25] that *in vivo* dose measurements should be made for every patient receiving radiotherapy. However, *in vivo* dosimetry is not a regular component of radiotherapy due to the additional cost and human resources needed[26].

For a dosimeter to be considered ideal for routine real-time *in vivo* dosimetry it has to meet the set of key requirements established by Rink *et al*.[27,28] It must be small enough to not shift tissue and should have an effective atomic number (Z_{eff} = 7.26[29]) similar to that of water in order to undergo similar interactions with ionizing radiation so as to not perturb dose distribution around it. It needs to have small volume over which dose is measured so as to not be susceptible to volume averaging in an area where dose distribution changes rapidly (known as *high dose gradient*, e.g. 6% drop per mm in brachytherapy type treatments), while being sensitive enough with sufficient signal to noise to measure dose down to 0.01 Gy. The dosimetric response should be acquired in real-time for intervention and correction during treatment. A full list of requirements is shown in Table 1. Some current commercially available dosimeters such as semiconductor silicon diode arrays, metal-oxide semiconductor field effect transistors, ion chambers and thermally/optically stimulated diodes have been adapted for *in vivo* dosimetry. However, these technologies have limitations such as size, atomic composition[30], temperature dependence[31] and pre-treatment

calibration[27,31] that preclude them for routine *in vivo* dose measures. Radiochromic film dosimeters have been suggested as a candidate that fulfills most of the aforementioned requirements[28,32].

Table 1: List of criteria for an ideal *in vivo* point based real-time dosimeter. Table recreated with permission. Rink *et al*[28], *Duterix *et.al*[33]

Criterion No.	Criterion	Comments
1	Small size (<1mm^3)	Does not physically perturb tissue and effect delivered dose to surrounding tissue; can measure point dose at interfaces between tissues of varying densities and composition; used on steep part of dose–depth curve or in the penumbra region; no build-up required for measurement
2	Near water-equivalent* (difference <10%) (response independent of energy)	Does not alter dose distribution to tissue (tissue assumed to be similar to water) * own reading converted to dose delivered to water (and/or tissue); does not cause artifacts during low energy image guided radiotherapy
3	Fast kinetics and stable response (interrogation process dose not induce false signal)	Both required for real-time readout of dose
4	Signal ∝ dose in 1-1000cGy range (linear within 2%)	Simplicity of conversion from measurements to dose; no need to track delivered dose to-date; simple function is acceptable in lieu of linearity
5	Dose resolution (down to cGy)	Measurements of doses down to a few cGy with relatively small errors (few %); suitable for IMRT
6	Dose-rate independence (10-1000 cGy/min) (no statistical difference using $\alpha = 0.05$)	No need for prior knowledge of dose; simplicity of measurements throughout the body
7	Insensitive to environmental conditions (<2% variation over clinical temperature range 20-38°C)	Temperature, humidity, and light insensitivity allows for easier incorporation and use within clinic
8	Nontoxic	Requirements of dosimeter embodiments are relaxed when medium contained within is nontoxic

1.3 Radiochromic film dosimetry

Radiochromic films are optical dosimeters that change in colour and increase in optical density when exposed to ionizing radiation[34]. Some radiochromic films, such as GafChromic® EBT-3 and MD-55 (Ashland, Bridgewater, NJ, USA) used for dosimetry, are composed of one or more sensor layers of radiochromic crystals suspended within a binder matrix such as gelatin[35,36]. The monomers composing the radiochromic crystals undergo polymerization when exposed to ionizing radiation without the need for chemical processing[34].

Commercial radiochromic films are typically used to measure two-dimensional dose distributions[34,37]. Because of their high spatial resolution, low energy dependence and near tissue equivalence (Z_{eff} = 7.26[29]), they are suitable for dose measurement in high dose gradients[34]. Dose measurements are typically performed 3-24 hours after exposure[38,39] due to polymerization taking place even after the end of exposure[27]. However, it was demonstrated by Rink *et al.* that radiochromic film dosimeters such as MD-55 and EBT (predecessor to EBT-3 with the same active component) can be used to measure dose in real time and *in vivo*[28,32] using a fiber-optic read-out and a spectrophotometer for measurements. The ΔOD measured during and at the end of exposure was still a predictable function of dose[28], and the post-exposure continuation of polymerization contributed minimal (~1%) uncertainty over clinically relevant doses and dose rates[40]. These advancements make radiochromic film dosimeters a strong candidate for real time *in vivo* dosimetry.

1.4 Background on radiochromic materials

The active component in radiochromic films intended for dosimetric purposes such as Gafchromic® EBT-3 and MD-55 (Ashland, Bridgewater, NJ, USA) is lithium-10,12-pentacosa diynoate (LiPCDA) and pentacosa-10,12-diynoic acid (PCDA), respectively[41]. Figure 2 shows the

chemical structure of both monomer units. These molecules are disubstituted diacetylene monomers with two side groups R_1 and R_2[28,36,42]. In the case of PCDA and LiPCDA, the R_1 group is a long carbon chain and the R_2 group has a carboxylate end group which is associated with either a H^+ or a Li^+.

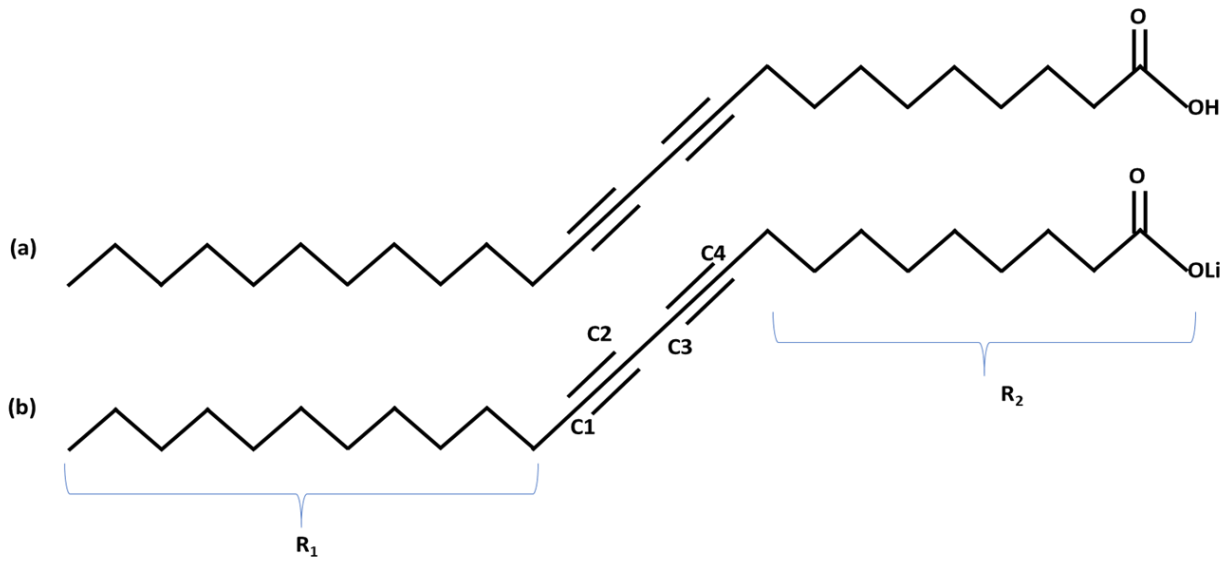

Figure 2: Chemical structure of monomeric PCDA (a) and LiPCDA (b)

Diacetylene monomers can self-pack into crystal structures[43] dependent on the size and composition of the side groups[36]. They can undergo *topochemical polymerization*[44–47], where the polymerization occurs only along one axis of the crystal. When exposed to ionizing radiation such as UV, X-rays and γ-rays the diacetylene monomers photopolymerize as a solid-state topotactic 1,4-addition reaction[46,48–50] first documented by Wegner in 1969[41,46,48]. The 1,4-addition reaction occurs due to radical formation when ionizing radiation is absorbed by the diacetylene monomer[45]. The mechanism responsible for the topochemical polymerization of disubstituted diacetylenes is known as the "turnstile" mechanism[47,52]. In the turnstile mechanism, diacetylene monomers pivot around the centroid of the diacetylene at 30°. This moves the C1 and C4 of the neighbouring

monomers approximately[39] 1 Å as the new bond is formed[47,52]. A schematic diagram of the monomer stacking, and polymerization are shown in Figure 3.

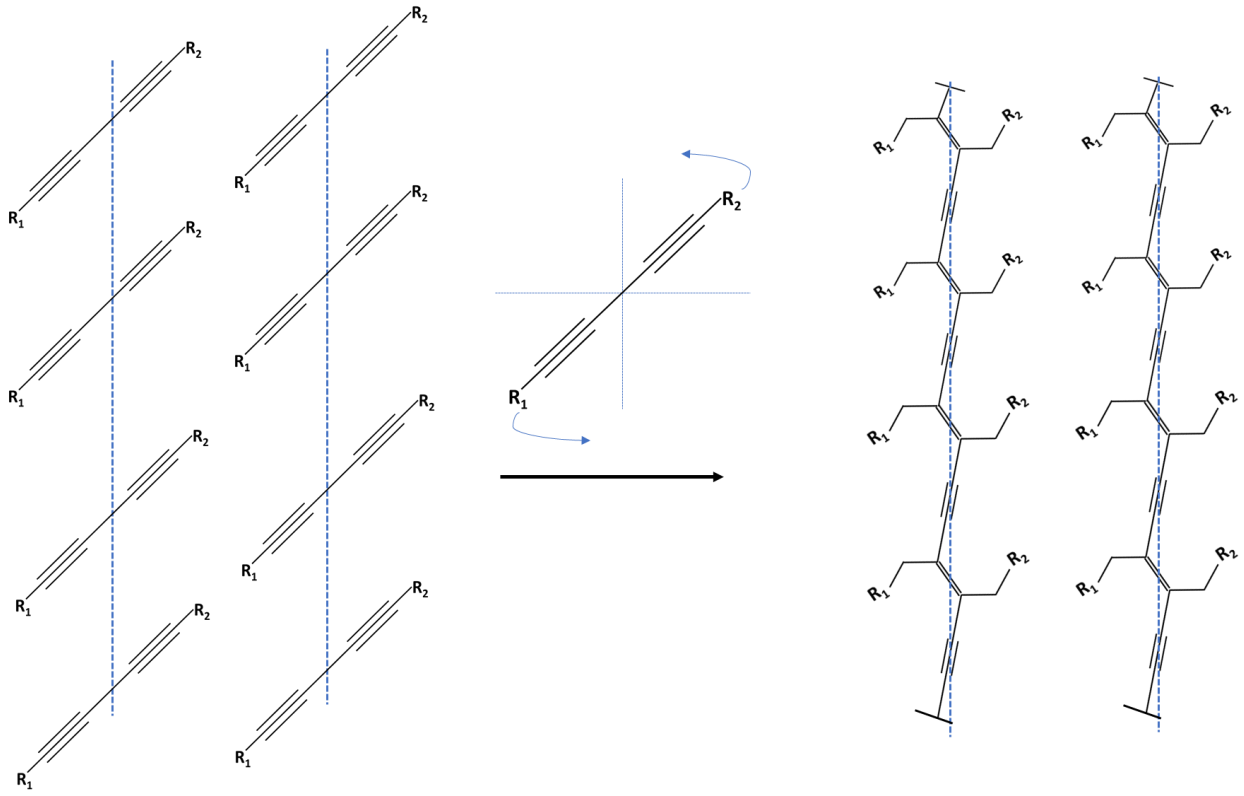

Figure 3: Schematic representation of the 1,4 topochemical addition reaction, the blue lines indicate the axis of polymerization.

This photopolymerization reaction leads to the formation of a polydiacetylene with alternating double (-ene) and triple (-yne) bonded carbon backbone[53]. The polymer formation is accompanied by a visible colour change, resulting in a change in absorbance (ΔA) which can be related back to the absorbed dose. The polymer formed has a deep color due to the lowest π electron transition of the conjugated polymer backbone[54]. As the ratio of polymer to monomer increases, the absorbance also increases[28,55]. Initially the polymer arrangement is constrained by the surrounding monomer matrix. As the polymer fraction increases the strain on the polymer structure due to the monomers is reduced[28,55]. The polymer then undergoes a slight reorientation dropping to a lower energy

state[28]. This lower energy state has a slightly shifted (few nm) absorbance peak relative to the constrained polymer[28,56,57]. In the case where all the monomers are polymerized and there are no constraints, the polymer undergoes a complete reorientation, accompanied by an abrupt large shift in absorbance peak and the polymer will turn red[58]. It was described by Enkelmann in 1984[44] that, for adjacent diacetylene monomers to react, they need to be packed in a ladder like configuration and within a distance less than or equal to the van der Waals contact distance, ~4 Å of each other[45,46,54]. The packing of monomers depends on the type and size of the end groups on the diacetylene[48,49]. The formed polymer backbone is composed of conjugated monomer units in a planar conformation[59]. The planarity of the backbone is also dependent on the R groups of the diacetylene, and the amount of strain applied to this backbone affects the colour of the polymer[59]. The formed polymer chain is shorter than the end-to-end distance of a monomer stack, thus when the diacetylene unit at the end of the polymer is too far from the adjacent monomer the reaction probability decreases and addition of subsequent monomers to polymer chain slows down and eventually terminates. This shortening of the polymer chain and reduced rate of monomer addition is the reason absorbance continues to increase even after the termination of irradiation. This post irradiation exposure darkening was reported to depend on the total dose delivered[60].

1.5 Recent findings of radiochromic film dosimetry

The dose response of a given radiochromic film is characterized by the net change in optical density (ΔOD_{net}) due to the polymer formation caused by ionizing radiation exposure. However, diacetylenes can have different dose response due to variation in packing, as described above. It has been shown that EBT (made of "hair-like" LiPCDA crystals, with an aspect ratio greater than with a length to width aspect ratio of 10:1[54]) has an 8-fold increase in dose sensitivity when compared to MD-55[32] even though the monomer only differs by a lithium ion associated at the

carboxylate end-group[54]. There are several other ways packing affects the response: location of main absorbance peak within the spectrum (λ_{max}), shift in λ_{max} with dose, and post-irradiation darkening[59].

MD-55 film (and others, including HD-810, MD-55-2, and HS) is composed of PCDA as the sensitive component which has a main absorbance peak (λ_{max}) occurring at 676 nm and a shoulder peak at 633 nm[28,62]. Klassen *et al.* have reported that PCDA has an linear increase ΔOD_{net} with dose between 0-6 Gy when using the main absorbance peak[63]. Whereas EBT (including EBT-2 and EBT-3) films, which use LiPCDA as their dose sensitive component with λ_{max} occurring at 635 nm and shoulder peak at 583 nm, are non-linear in dose response[32,64,65]. The dose response of these films has also been investigated using wavelengths outside of the main absorbance peak, which allowed for measurement of dose up to 100 Gy[66]. Raman spectroscopy has been used to investigate the packing of polydiacetylenes[67] and measure absorbed dose[68], but is not a practical solution for real-time dosimetry given the required instrumentation and complexity for these measurements.

A shift in λ_{max} to shorter wavelengths was observed for MD-55[56] as the absorbed dose was increased. This was not the case for EBT as the λ_{max} is stable with increased dose[32]. The percent increase in EBT's post-exposure ΔOD was also found to be nearly two times lower than MD-55 which may indicate that the polymerization kinetics of LiPCDA are faster than PCDA[32]. These differences are suggested to be due to the packing of the monomers[32], where association with the Li^+ may change the separation distance between the PCDA monomers[69]. The stability of the main absorbance peak and the faster kinetics suggest that the monomers in EBT are more stable following a polymerization and that there is no significant change in separation distance between the un-polymerized monomers and polymerized monomer units[32].

Other research groups have also looked at the molecular packing of PCDA through X-ray diffraction of PCDA Langmuir-Blodgett films[70]. It was found that different cations present in the subphases could impact the molecular packing and by extension the monomer separation of PCDA which was reflected in the X-ray diffraction profiles[70]. PCDA has also been shown to form photoreactive cocrystals which are also radiation sensitive[71]. The cocrystal variations of PCDA showed differences in their translational repeat distance and inter-alkyne distance which were accompanied by altered sensitivity to UV irradiation[71]. These findings show that the radiation response of diacetylenes can be influenced by altering the monomer spacing through incorporating small molecules in the monomer crystal rather than solely through monomer chemistry.

It has been shown that LiPCDA crystals can exist in two forms: the “hair-like” structure in commercial EBT films (635LiPCDA) and an alternate form with an absorbance peak occurring at ~674nm [54] (674LiPCDA). The 674LiPCDA form can be achieved by making "plate-like" crystal structures of LiPCDA (similar to PCDA) having an aspect ratio of less than 2:1, or through desiccation of 635LiPCDA[54]. The latter was suggested to have resulted in a twisting of the conjugated polymer backbone[59,72], evidenced by the spectral shift from 635 nm to 674 nm, due to the potential change in the packing of the monomers. This situation is somewhat unique given that packing of diacetylene monomer units typically depends on the R_1 and R_2 end groups which were not changed.

1.6 Hypothesis

It is hypothesized that the dosimetric behaviour of radiochromic crystals are primarily dependent on structure, which may be a function of more than just the chemical composition of individual monomers. Specifically, without changing the chemistry of the monomers of LiPCDA the dose response may still be altered through a difference in packing structure and monomer

separation by removing a small molecule, that of water, that was incorporated into the crystal. The resulting 674LiPCDA is expected to have a similar dose response to PCDA: linear and less sensitive to dose compared to 635LiPCDA, with greater post-exposure darkening.

Chapter 2: Dosimetric evaluation of a modified EBT-3 radiochromic film

2.1 Introduction to evaluation of modified EBT-3

This chapter describes the effect of desiccating 635LiPCDA to 674LiPCDA on radiochromic film's dosimetric behaviour. Because of the decrease in ΔOD_{net} per dose, films composed of 674LiPCDA should exhibit an increase in dynamic range compared to commercial EBT-3 film which has optimal signal response between 0.2Gy and 10Gy[73]. An overlap in dynamic range may allow for a two-point verification of dose since the two crystal forms have separate absorbance peaks[54]. In this chapter, the methods used to investigate this hypothesis are described in detail.

2.2 Materials and methods

2.2.1 Solid Water^{TM} Phantom

For real-time measurements, a custom 30 cm x 30 cm x 4 cm Solid Water^{TM} phantom, which has X-ray attenuation similar to that of water, and optical fiber read-out was used [74]. The films were positioned in the center of the custom phantom with the centre of the film (and point of optical read-out) at 1.5 cm depth along the irradiation beam's central axis. Two removable optical fiber holders also made from Solid Water^{TM} were embedded in the phantom, holding the optical fibers at 1.5 cm depth in the phantom perpendicular to the film for transmission spectroscopy. A ~50 cm (1500/1550 core-cladding diameter in μm, Thorlabs, Newton, NJ, USA) fiber is used to deliver light to the film and an identical fiber was used to collect transmitted light, as shown in Figure 4. The delivery and detection fibers have a non-connectorized bare fiber end inside the solid water phantom. In this configuration the light was transmitted from the delivery fiber through the film and collected by the detection fiber, in semi-free space; the holders were used to line up and inhibit motion in the system. The phantom allowed for replacement of film samples, by using a removeable film holder with holes for polished bare optical fiber, made from

the same material. The film holder had a switchable component which could hold either one or two ~1 cm x 1 cm commercial films.

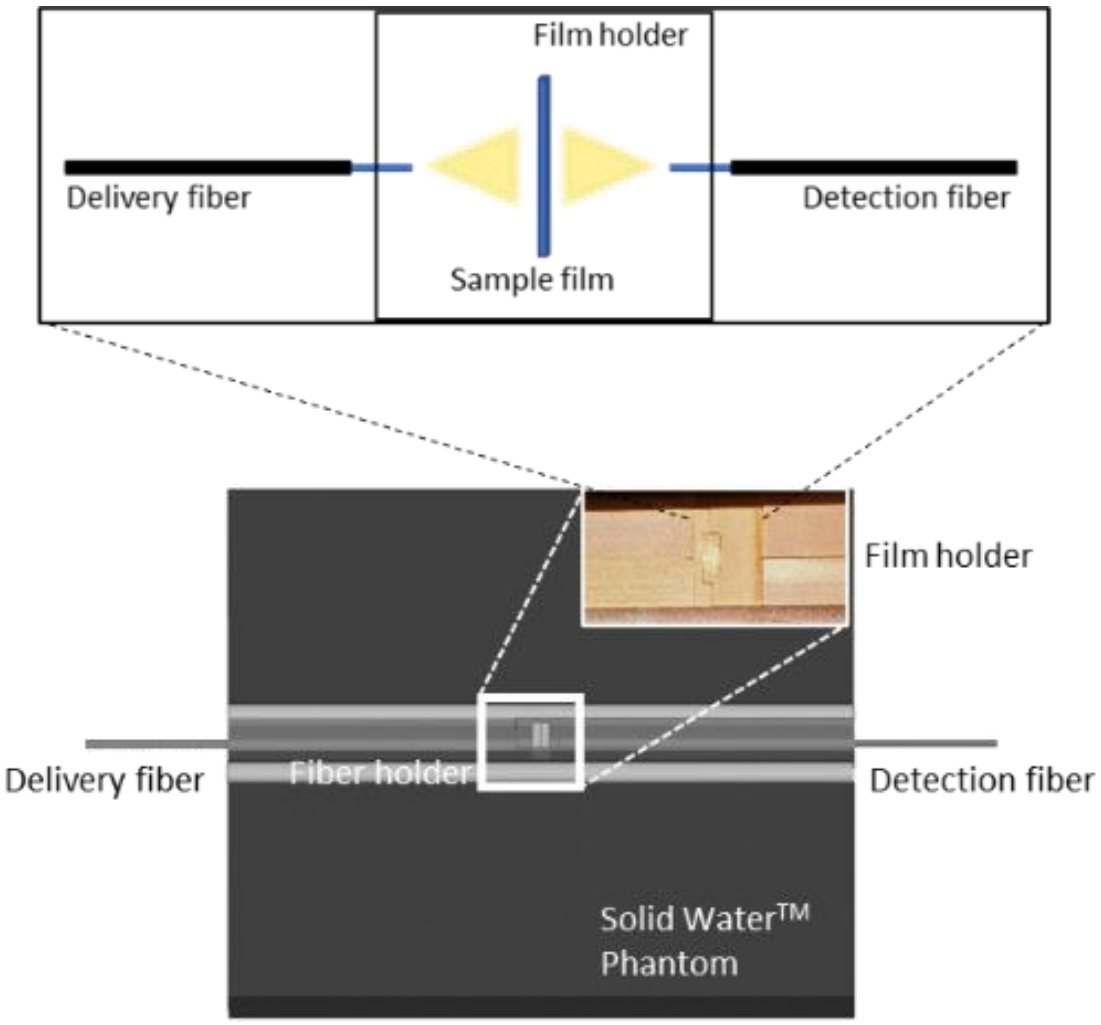

Figure 4: Schematic diagram of the custom phantom showing the fiber and film holders embedded into the phantom, with delivery and detection fibers protruding from the phantom. A magnified view of the film holder demonstrates the light path through the sample film.

2.2.2 Modification of EBT-3 film

EBT-3 film is comprised of an active layer that is reported to be 27 μm thick sandwiched between two 120 μm transparent polyester substrates[75]. For a comparative investigation, both 635LiPCDA and 674LiPCDA were sourced from a single sheet of commercially available EBT-3

film (lot No. 03111902), cut into two halves. One half, was left unaltered and stored in a light safe box, acting as the reference sample of 635LiPCDA. The second half had one substrate layer peeled off to expose the radiochromic coating. The peeled film was then desiccated in an oven at 45°C with ~10 g of calcium chloride desiccant over ten days. This film is referred to as DesEBT-3. Both films were stored in a light safe box until exposure experiments with a LINAC. At the time of experiments, randomly selected segments ~1 cm x 1 cm were cut out of EBT-3 and DesEBT-3 films for irradiation. This was done to avoid any coating biases such as minor differences in thickness of the film due to coating direction.

2.2.3 Scanning Electron Microscope imaging

To prepare the films for SEM imaging, a 5 cm x 5 cm (each subdivided further into ~ 1cm x 1cm pieces) film sample was cut from both the EBT-3 and DesEBT-3 films. These were placed into separate beakers with ~30 ml of water. The beakers with the films were then put in a hot water bath at ~45°C (below the melting temperature of the crystal) and stirred for 2–3 hours. This process melted the binder material and separated the active component from the polyester substrate. The polyester pieces were picked out, and the remaining contents of each beaker were then poured onto filter paper (Whatman™, particle retention >11μm) and left in an open environment for 3–4 days. The polymer crystals of LiPCDA, which are water insoluble, were then scraped off the filter and placed onto SEM stubs for imaging. Both 635LiPCDA and 674LiPCDA were imaged with a scanning electron microscope (SEM, Quanta™, Thermo Scientific™, Waltham, MA, USA) in a high vacuum and with an accelerating voltage of 10 kV.

2.2.4 Dose delivery and ΔOD measurement

For exposure experiments, the film samples were put inside the Solid Water™ phantom. The phantom was then placed on top of at least 10 cm of backscatter, which was placed on the

patient bed of a Varian True Beam linear accelerator (Varian Medical System, Palo Alto, California, USA). The film inside the phantom was positioned at the center of the beam using its crosshairs. All films were irradiated with a 6 MV beam under standard conditions (100 cm source-to-axis distance, 10 x 10 cm field of view). A range of doses between 50 –7000 cGy in total dose were delivered at 300 cGy/min. Five film samples were used from both EBT-3 and DesEBT-3 for every dose up to 3000 cGy. Only DesEBT-3 was exposed to doses greater than 3000 cGy.

The light source used to measure radiation induced change in optical density was a broad spectrum (360–2400 nm) tungsten halogen source (5W HL-2000-FHSA, Ocean Optics Inc., Orlando, FL, USA). The light source was located outside of the radiation bunker and connected to a 17 m long fused silica fiber (600/630 μm core-cladding diameter, Thorlabs, Newton, NJ, USA). The long fiber was then then pulled through the radiation bunker and SMA connected to the delivery fiber. Another 17 m long fused silica fiber (600/630 μm core-cladding diameter, Thorlabs, Newton, NJ, USA) was SMA connected to the detection fiber and returned from the phantom to a spectrophotometer outside the bunker. The spectrophotometer used for detection was a 200–1100 nm range CCD camera (USB4000, Ocean Optics, Orlando, FL, USA). The spectrometer integration time was varied between 10–80 ms, depending on the experiment; however, the frequency of spectra collection was maintained at ~1 Hz for all experiments. Post-exposure development experiments were completed by continuously measuring the absorbance spectra of 5 film samples of each crystal form, for ~60 min after 200 cGy dose exposure. A schematic diagram of the complete measurement apparatus is shown in Figure 5.

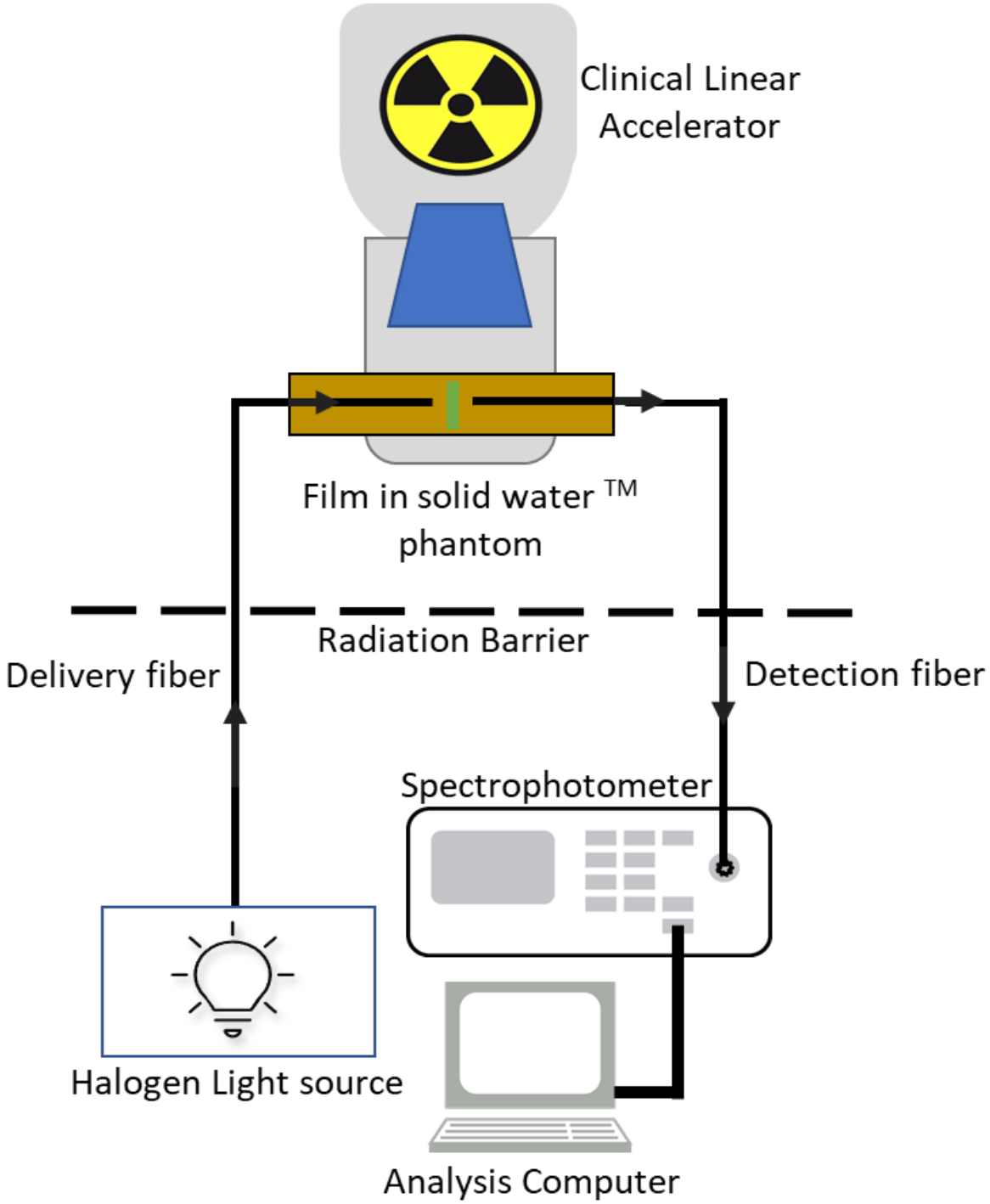

Figure 5: Schematic diagram of the real-time X-ray exposure apparatus. The light to and from the phantom is transported through the radiation barrier through 17 m fused silica fibers.

Spectral data were analyzed using a MatLab® based software. Transmitted light through the film sample was measured prior to, during and after exposure. The light measured before

irradiation was used as the background or reference spectrum. The Δ*A* was calculated as the log of the ratio of the light transmitted through the film sample before exposure and the transmitted light during and after exposure as described by equation 1.

$$\Delta A(\lambda) = log_{10}(\frac{I(\lambda)_{ref} - I(\lambda)_{dark}}{I(\lambda)_{data} - I(\lambda)_{dark}}) \quad (1)$$

where $I(\lambda)_{ref}$ is the background reference intensity collected before the X-ray beam was turned on, $I(\lambda)_{dark}$ is the dark spectrum which accounts for stray light collected by the spectrophotometer with no interrogation light being allowed to reach the detector, and $I(\lambda)_{data}$ is the transmitted light intensity collected during and after exposure. The ΔOD, as shown in equation 2, is then calculated by integrating the absorbance 10 nm around the main absorbance peak of the sample film[54,74] where λ_n to λ_1 spans the 10 nm window. This averaging window was used to minimize the errors associated with λ_{max} occurring at slightly different wavelengths due to system noise[28,32].

$$\Delta OD \equiv \frac{1}{\lambda_n - \lambda_1} \sum_{i=1}^{n-1} \left(\frac{\Delta A_i + \Delta A_{i+1}}{2} \right) (\lambda_{i+1} - \lambda_i) \quad (2)$$

A schematic plot in Figure 6 shows that the net optical density as a function of time can be broken up into three distinct sections: (a) pre irradiation, (b) during irradiation, and (c) post-irradiation. The ΔOD at end of radiation, marked by an abrupt change in ΔOD increase, is used to determine the comparative change in optical density with dose for each sample. The uncertainty in average ΔOD is reported as a percent standard deviation (%σ), determined by equation 3.

$$\%\sigma = \frac{\langle \Delta OD \rangle}{\sqrt{\frac{\sum_i^n (\Delta OD_i - \langle \Delta OD \rangle)^2}{n-1}}} \quad (3)$$

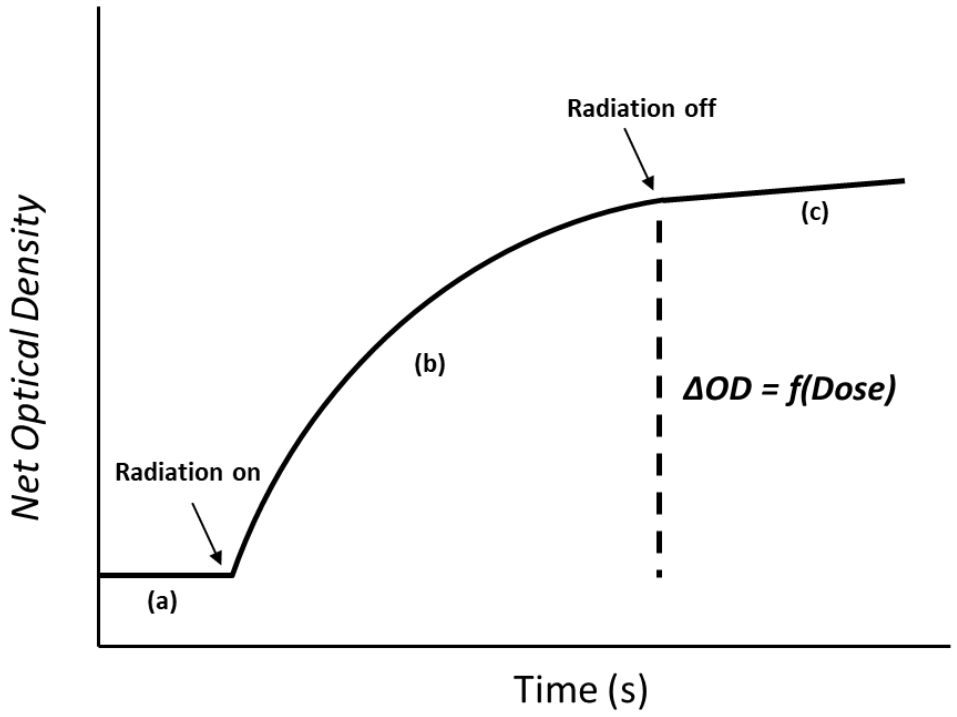

Figure 6: A model representation of the optical density change as a function of time. The irradiation is applied for a period of time depicted by segment (b).

By plotting the ΔOD against total dose, calibration curves for both DesEBT-3 and EBT-3 were generated. The dose curves of each film around the main absorbance peak are expected to be a third order polynomial function[40,76] of the form shown in equations 4 and 5,

$$\Delta OD_{DesEBT-3}^{\lambda_n-\lambda_1} = p1(D)^3 + p2(D)^2 + p3(D) + p4 \quad (4)$$

$$\Delta OD_{EBT-3}^{\lambda_n-\lambda_1} = p5(D)^3 + p6(D)^2 + p7(D) + p8 \quad (5)$$

where *D* is the total dose in cGy delivered and *p1–p8* are coefficients determined experimentally by fitting the polynomial to the calibration curves.

The post-irradiation segment (c) depicts increased optical density growth between the time of irradiation completion and end of measurement. The percent increase in OD after the point of end of radiation is referred to as post-exposure kinetics and is used as a surrogate measure of kinetics during exposure. This is required because during a beam segment the propagation of polymers and initiation of new polymerization reactions are simultaneously taking place, both contributing to the increased optical density, with no way to separate the two without extensive modeling. Thus, the percent increase in OD was measured for ~1 h after exposure for both 635LiPCDA and 674LiPCDA with five film samples each. Films were exposed to 200 cGy delivered with a 6 MV beam at 300 cGy/min, data was continually collected before, during, and ~1 h after irradiation.

2.2.5 Multifilm dose measurement

Since both 674LiPCDA and 635LiPCDA are dose sensitive and have spectrally resolvable absorbance peaks, a two-point verification of total dose delivered is possible. In a simplest iteration, both 635LiPCDA and 674LiPCDA can be placed in direct contact with each other in the film holder. In this case, they can be assumed to be at the same point in space for dose measurements and exposed to the same total dose. The light path is directed through both films from the delivery fiber to the detection fiber. Since the interrogation light travels through both films, the absorbance of each film is additive. Thus, the dose response or total change in optical density is give by equation 6,

$$\Delta OD^{\lambda_n-\lambda_1}_{measured\ total} = \Delta OD^{\lambda_n-\lambda_1}_{EBT-3} + \Delta OD^{\lambda_n-\lambda_1}_{DesEBT-3} \quad (6)$$

where the $\Delta OD^{\lambda_n-\lambda_1}_{measured\ total}$ is the change optical density measured for the combined absorbance spectra calculated using equation 2. Then by substituting the dose curves of each film shown in equation 4 and 5, the total dose is determined by solving the third order polynomial shown in equation 7. Solutions to equation 7 are then determined iteratively using the fitted coefficients.

$$0 = (p5 + p1)(Dose)^3 + (p6 + p2)(Dose)^2 + (p7 + p3)(\text{Dose}) - (\Delta OD^{\lambda_n-\lambda_1}_{measured\ total} - p4 - p8) \quad (7)$$

The combined films were exposed to 100–3000 cGy using a 6MV beam at 300 cGy/min dose rate.

2.2.6 Growing crystals of 674LiPCDA

LiPCDA monomers were also chemically varied by changing the concentration of Li^+, to determine if a similar spectral shift would be observed. A concentration series of Li^+ was prepared by varying the molar ratio of Li^+ to PCDA from 0.2:1 to 1:1. Absorbance spectra after exposure to UV light were then measured, and SEM images of these formulations coated on to Mylar film were obtained.

2.3 Results and discussion

2.3.1 Comparison of absorbance

Absorbance spectra of reference EBT-3 film and DesEBT-3 after 5 Gy dose are shown in Figure 7 and demonstrates that most, or all, of 635LiPCDA crystals have been converted to the 674LiPCDA form. The fraction of water removed from the film through desiccation was not quantified. The peak absorbance for reference EBT-3 film occurred at the expected wavelength of ~635 nm. DesEBT-3 peak absorbance occurred at ~674 nm with a shoulder peak at ~620 nm,

similar to PCDA[28,63]; however, the peak absorbance was much lower in comparison to 635LiPCDA.

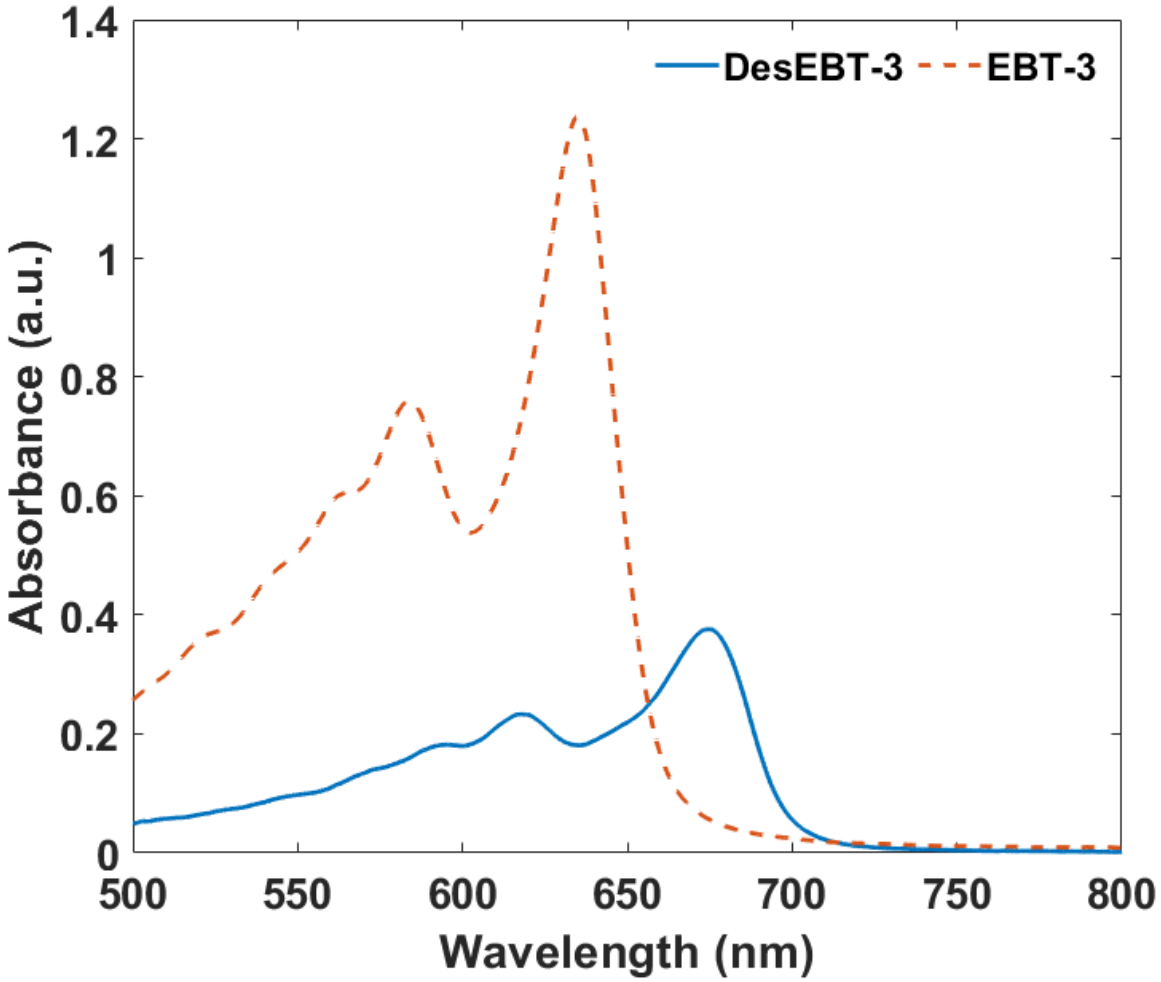

Figure 7: Change in absorbance of DesEBT-3 (674LiPCDA) and reference EBT-3 (635LiPCDA) film. Films were exposed with a 6MV x-ray beam at a rate of 300 cGy/min to a total dose 500 cGy.

This confirms that the commercial EBT-3 film consisting of 635LiPCDA crystals can be reliably converted to the 674LiPCDA form through desiccation. The shift in absorbance spectra indicates that the molecular electronic configuration has changed and that removal of water had caused a twisting of the backbone, as previously suggested[54].

Absorbance spectra of formulated crystals showed, that a 1:1 ratio of Li^+ to PCDA resulted in a LiPCDA polymer, which has absorbance spectrum similar to 674LiPCDA. In contrast, a 0.2:1 stoichiometric ratio has a spectrum like that of 635LiPCDA. This suggests that in 635LiPCDA of commercial EBT films is likely a mixture of Li^+ and H^+ associated diacetylene monomers.

2.3.2 Macroscopic crystal structure comparison

It has been shown that 674LiPCDA crystals can be grown instead of being produced through the conversion of 635LiPCDA[54]. When the 674LiPCDA crystals are grown, they demonstrate a "plate-like" structure with an aspect ratio less than 2:1, similar to PCDA. However, when the 635LiCPDA crystals present in EBT-3 films were desiccated and demonstrated a spectral shift, their crystal morphology did not show any notable difference compared to the un-desiccated 635LiPCDA crystals. The 674LiPCDA produced through desiccation maintained an aspect ratio greater than 10:1. Electron micrographs (Figure 8) show a qualitative comparison of the overall structures at 2500x magnification and 10.00 kV accelerating voltage. The 674LiPCDA crystals maintain their shape and size, with no notable fragmentation due to the desiccation even when viewed at 25,000x magnification. This suggests that the absorbance shift is likely due to changes in the molecular packing of the monomers at the microscopic scale, which does not alter the macroscopic crystal structure. In contrast, SEM images of formulated crystals (Figure 9) show different crystal morphologies, where the 1:1 LiPCDA (absorbance peak at 674 nm) is "plate-like" and the 0.2:1 LiPCDA (absorbance peak at 635 nm) has a "hair-like" crystal morphology. This indicates that the Li^+ concentration can influence which of the two LiPCDA crystal structures is formed.

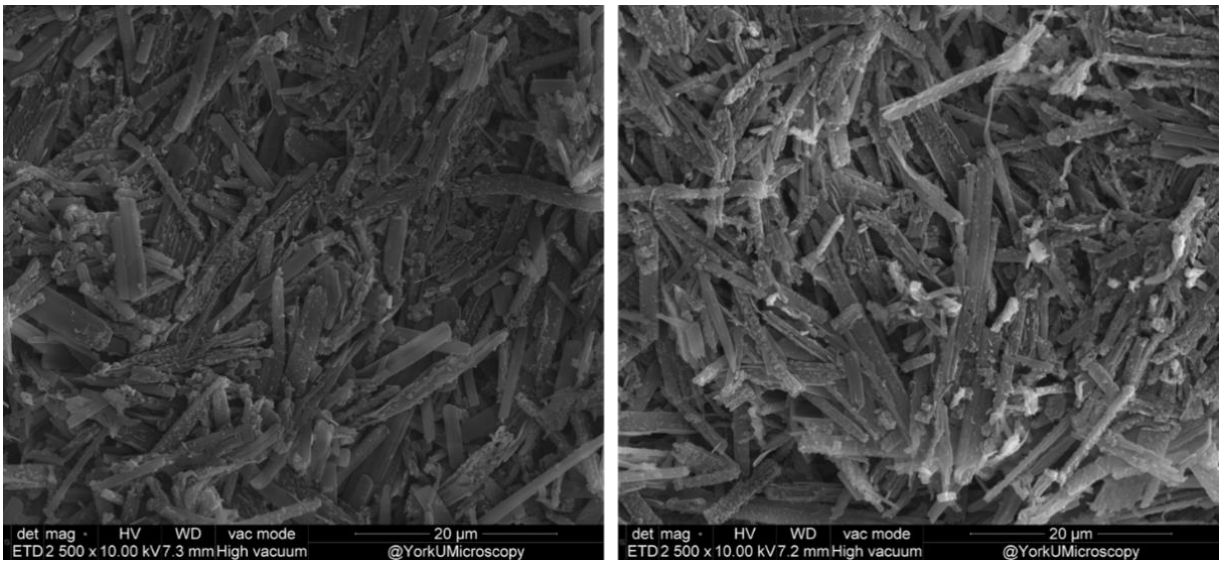

Figure 8: SEM images of DesEBT-3 (674LiPCDA) (left) and EBT-3 (635LiPCDA) (right) with binder removed. Images were taken at 2500x magnification.

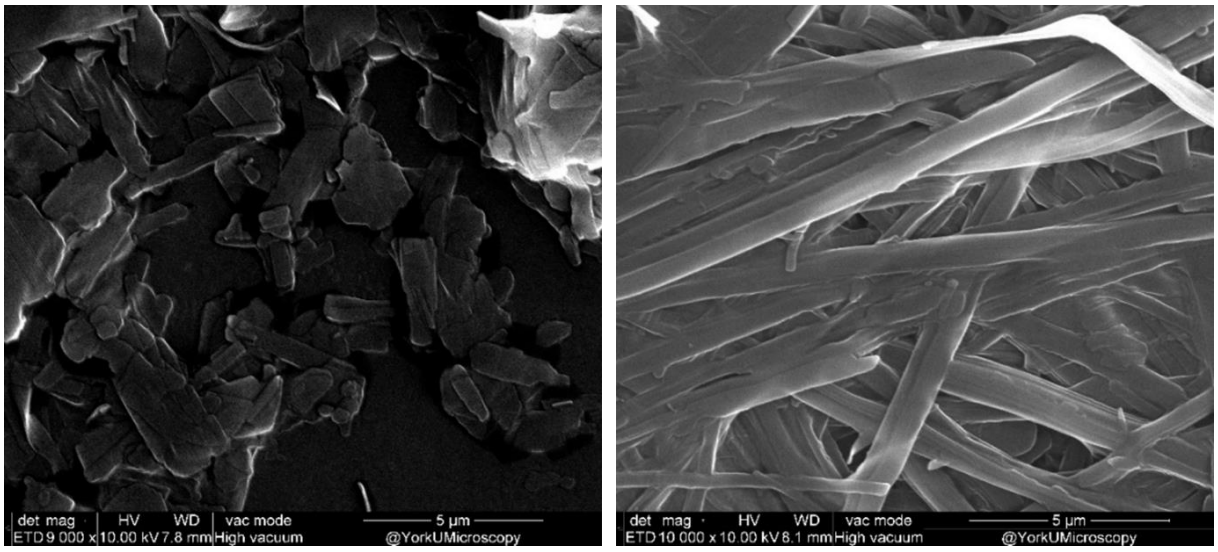

Figure 9: SEM images of "plate like" LiPCDA (left) and "hair-like" LiPCDA (right). Images were taken at 9000x and 10000x magnification for "plate-like" and "hair-like", respectively.

In a recently published thesis[77], thermogravimetric analysis and solid state NMR results showed that the 635LiPCDA is a LiPCDA monohydrate while 674LiPCDA is anhydrous LiPCDA. This corroborates our findings that the water content is an integral part of the crystal structure of LiPCDA.

2.3.4 Evaluation of dose-response of DesEBT-3

674LiPCDA obtained through desiccation has dose sensitivity ~3x lower than commercial 635LiPCDA. The ΔOD_{net} against dose is shown in Figure 10 and Table 2 contains a summary of the percent standard deviation based on five separate samples for each film at all nominal total doses. When commercial EBT-3 films were exposed to doses >20 Gy, a diminished ΔOD_{net} was observed as absorbance started to reach the saturation limits of the spectrophotometer (ΔOD > 2.5). It was expected that 674LiPCDA films would have a linear dose response similar to PCDA, up to 6 Gy using the main absorbance peak (λ_{max} = 676 nm)[63] however, no linear dose response was observed between 0-70 Gy. The lower dose response of 674LiPCDA films allowed for signal detection at higher doses, up to 70 Gy and potentially higher. The high uncertainty (%σ standard deviation) measured for DesEBT-3 may be due to the incomplete desiccation of 635LiPCDA.

A shift in λ_{max} for 674 LiPCDA (Figures 11 and 12) was observed with increasing dose. This shift from 677 ± 1.1 nm to 674 ± 0.5 nm occurred when 674LiPCDA was exposed to doses >500 cGy. In contrast, 635LiCPDA maintained a constant λ_{max} up to the saturation limit of 2000 cGy. The shift in λ_{max} indicates that the polymer may have undergone a reorientation and that the monomers in 674LiPCDA are not in their most stable configuration. Thus, as the dose is increased, and the polymer rearranges the monomer separation changes resulting in a shift in λ_{max}.

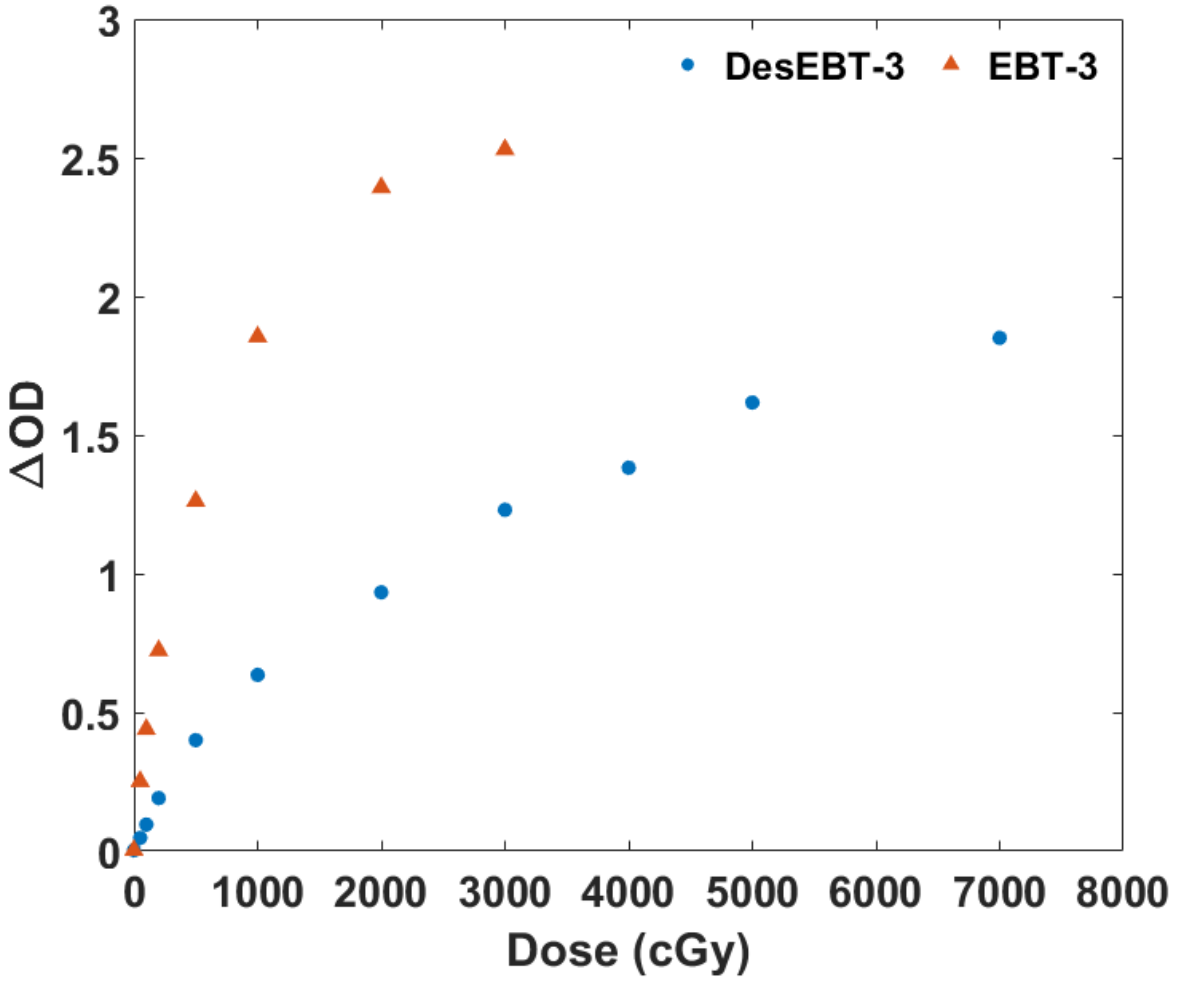

Figure 10: ΔOD as a function of dose for EBT-3 (635LiPCDA) and DesEBT-3 (674LiPCDA) films. EBT-3 films were exposed to 50–3000 cGy, reaching detection limits between 2000–3000 cGy. DesEBT-3 films were exposed up to 7000 cGy,

Table 2: Percent standard deviation (%σ) of dose measurement with N=5 independent samples.

Dose (cGy)	50	100	200	500	1000	2000	3000	4000	5000	7000
%σ EBT3	1.4	0.7	0.4	0.8	0.6	0.2	0.4	-	-	-
%σ Des EBT3	4.9	2.6	1.5	1	2.8	1.9	2.2	2.2	1.5	0.5

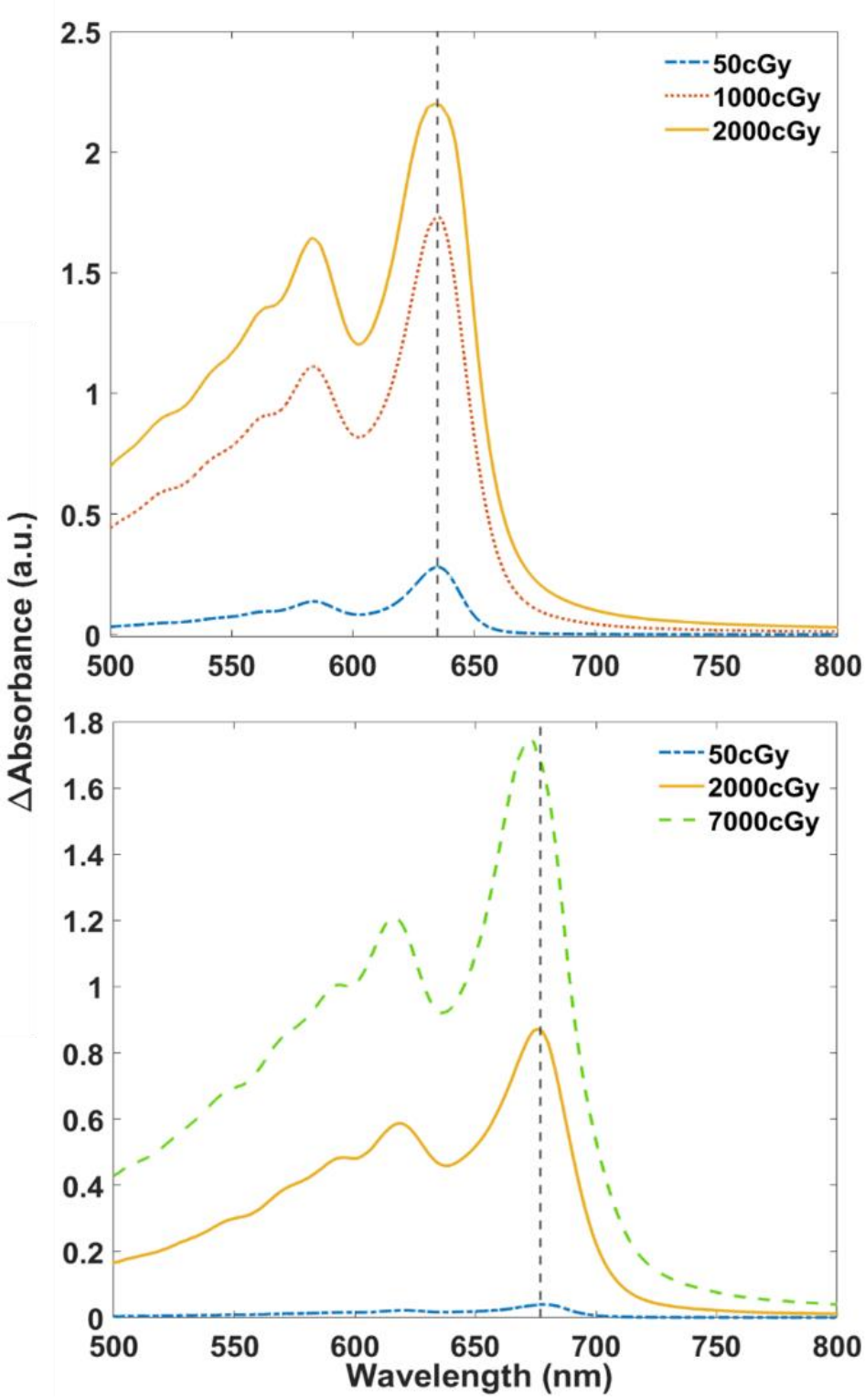

Figure 11: Sample absorbance spectra of 635LiPCDA (top) and 674LiPCDA (bottom) with vertical dashed line at 635 nm and 677 nm respectively, spectra were collected at the end of exposure.

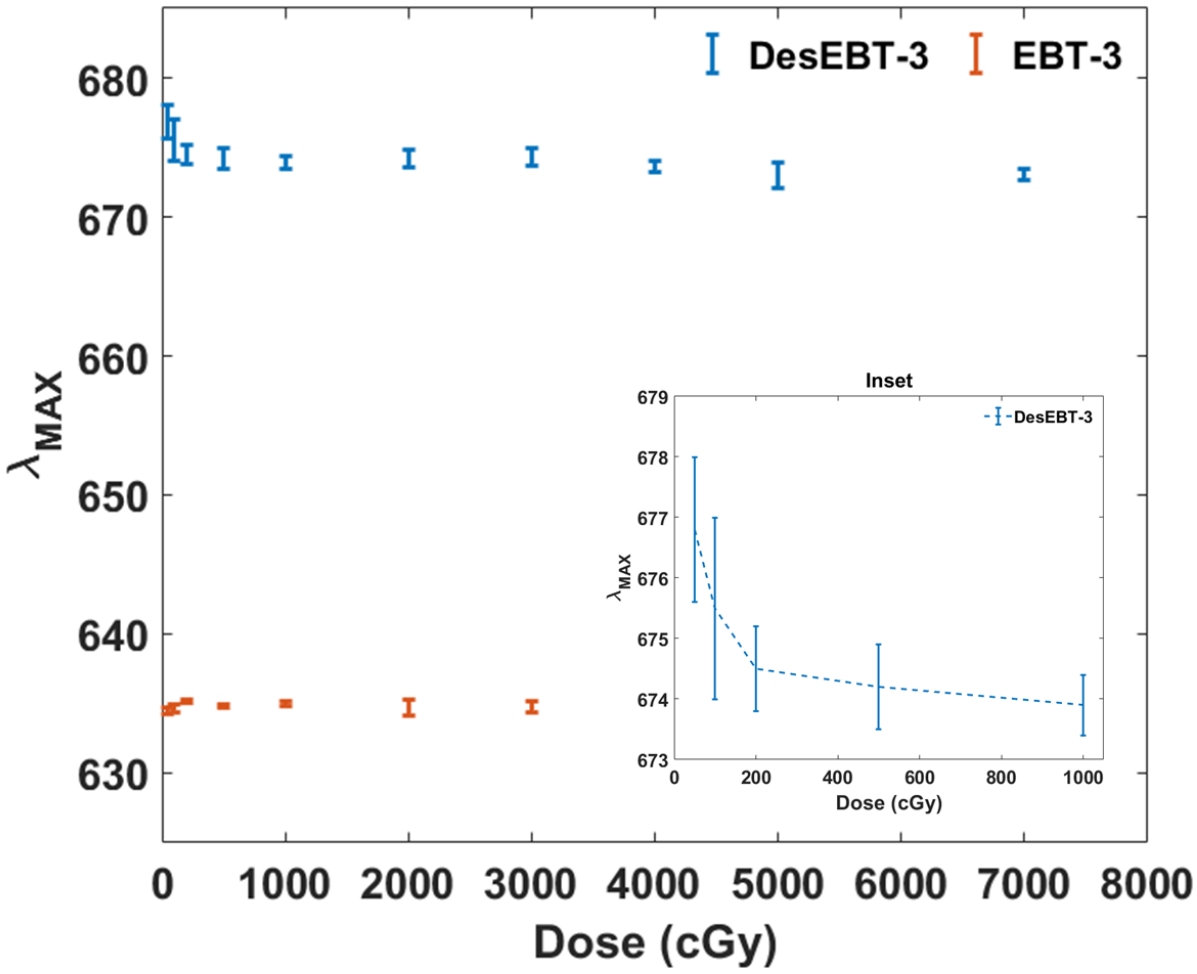

Figure 12: Wavelength at peak absorbance against total dose delivered, N=5 film samples were exposed for each nominal dose. Error bars represent 1σ standard deviation. Inset figure shows the initial decrease in λ_{max} with dose of DesEBT-3.

2.3.5 Post-exposure response

The post-exposure continual development of radiochromic film is a potential point of concern for real-time dosimetry[28,60]. Due to difficulties in teasing out this information during irradiation, this is assessed by measuring the extent of OD increase after end of exposure as a function of time[28]. Figure 13 shows the percent increase in OD over time after exposure to 200 cGy for a single sample of EBT-3 and DesEBT-3.

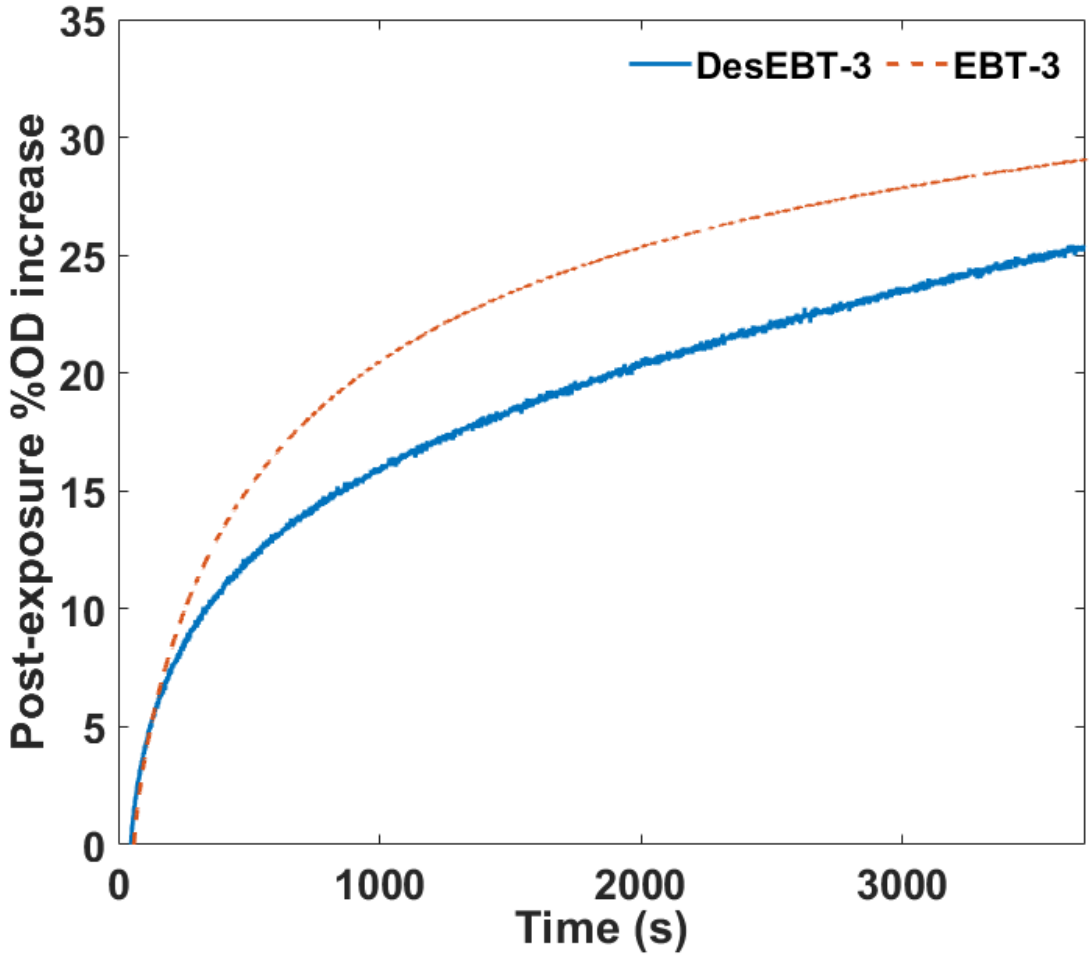

Figure 13: Percent post-exposure OD increase for N=1 sample, exposed with a 6 MV beam to 200 cGy at a 300 cGy/min. Data was continually collected for ~1 h after exposure.

A summary of the post-exposure percent increase in OD for both films, along with p-values, are shown in Table 3. Results show an average (N=5 independent samples) of 5.0 ± 0.1 % increase in OD after 1 min and 29.2 ± 0.3% after 60 min following exposure for 635LiCPDA, while the 674LiPCDA had a 3.7 ± 0.1 % at 1 min and 25.2 ± 3.8 % after ~1 h. A t-test to compare means at ~1 h with $\alpha = 0.05$ resulted in a two tailed p-value > 0.05, indicating that the post-exposure kinetics of 635LiCPDA and 674LiPCDA are not significantly different at 1 h. However, at times <1 h, the percent increase in OD was greater for 635LiPCDA. The <1 h values indicate that the

polymerization kinetics of the 674LiPCDA may be faster than 635LiPCDA. This was an unexpected result given that 635LiPCDA previously showed faster polymerization than PCDA[30] and we believed PCDA to pack similarly as desiccated LiPCDA. To make a definitive conclusion, repeat post-exposure data needs to be collected over a longer period of time (>1 h). A high amount of uncertainty (%σ standard deviation) was recorded for average %OD increase for DesEBT-3, possibly due to incomplete desiccation as previously mentioned.

Table 3: Post-exposure kinetics of both 635LiPCDA and 674LiPCDA with N=5 samples averaged at specific time points after exposure. P-value indicates the statistical difference in %OD increase between both film formats for each time point (α =0.05)

Time (min)	<%OD increase> EBT-3	<%OD increase> DesEBT-3	P-Value
1	5.0 ± 0.1	3.8 ± 0.1	5.9×10^{-7}
5	13.3 ± 0.3	9.6 ± 0.6	2.6×10^{-5}
10	18.2 ± 0.4	12 ± 1	2.4×10^{-4}
15	21.1 ± 0.5	15 ± 2	5.7×10^{-4}
30	25.7 ± 0.6	20 ± 3	6.5×10^{-3}
60	29.9 ± 0.6	26 ± 4	9.7×10^{-2}

2.3.5 Clinical application

A radiochromic probe dosimeter for real-time *in vivo* use needs to be sensitive to low dose, as described in Table 1. But ideally it would also have a dynamic range above 10 Gy for applications in brachytherapy which can have prescribed doses of 13–19 Gy, and hyper doses of 200–400% of that. In stereotactic radio surgery, the prescribed dose per fraction can be 8–30 Gy[78]. Since 635LiPCDA radiochromic dosimeters have a dynamic range of 0.1–20 Gy, depending on the spectral range being used, this material alone is limited to only some applications. A potential novel way to increase the dynamic range of a radiochromic fiber optic probe dosimeter is to use both 635LiPCDA and 674LiPCDA in a single coating. The absorbance spectra of the combined

films and independent films are shown in Figure 14. This combined dosimeter can potentially have the high dose sensitivity of 635LiPCDA at low doses and extend the dynamic range with 674LiPCDA above 20 Gy.

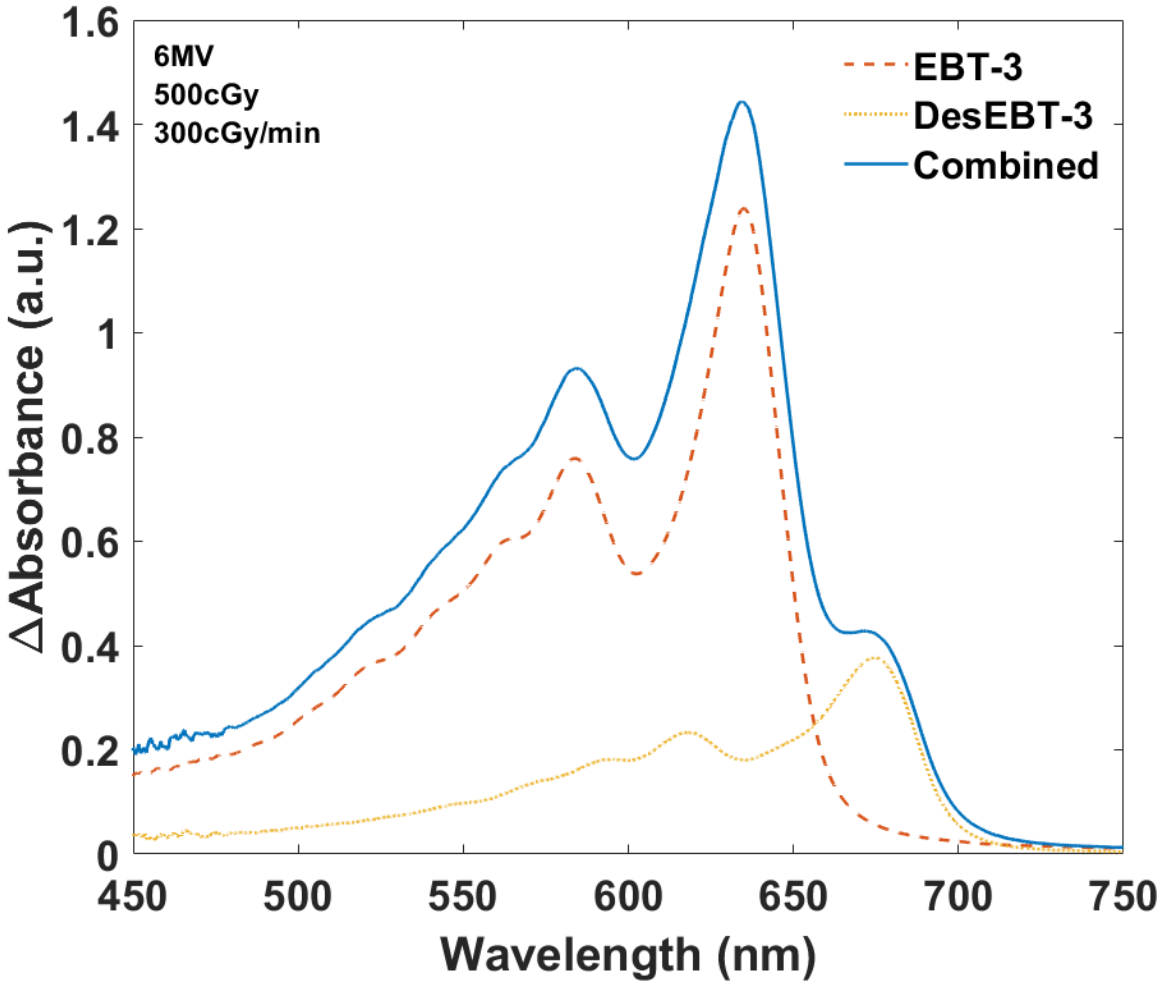

Figure 14: Absorbance spectra of combined 635LiPCDA and 674LiPCDA films (solid) and independent measures of 635LiCPDA (dash) and 674LiPCDA (dash-dot) after exposure to 500 cGy with a 6 MV beam at a 300 cGy/min.

The algorithm described in section 2.6 for multi-film measurements was able to determine the true dose delivered up to 500 cGy within 1% error, when using the 630–640 nm absorbance window as shown in Table 4. At doses close to 10 Gy and above, the algorithm would significantly

underreport dose due to the detector saturation for combined 635LiPCDA and 674LiPCDA in this part of the spectrum. To report dose more accurately above 500 cGy using two films, the wavelength range was shifted to 670–680 nm which is ~10 nm around the peak absorbance of 674LiPCDA. When using the 670–680 nm absorbance range to determine the ΔOD, it was found that the polynomial coefficients p_1 and p_2 shown in equation 6 tend to 0 ($p_1 \to 0, p_2 \to 0$). Thus, in the absorbance window of 670–680 nm the dose response of 635LiPCDA was reduced to a linear function of the form shown in equation 8.

$$\Delta OD_{EBT-3}^{630-640} = p_1(D)^3 + p_2(D)^2 + p_3(D) + p_4 \quad (8)$$

$$\Delta OD_{EBT3}^{670-680} = p_5(D) + p_6 \quad (9)$$

$$\Delta OD_{DesEBT-3}^{630-640} = p_7(D)^3 + p_8(D)^2 + p_9(D) + p_{10} \quad (10)$$

$$\Delta OD_{DesEBT-3}^{670-680} = p_{11}(D)^3 + p_{12}(D)^2 + p_{13}(D) + p_{14} \quad (11)$$

Where p_5 and p_6 are determined by curve fitting a linear regression on to the dose against ΔOD data. Table 4 contains a summary of calculated dose using different spectral bands against the actual dose delivered. The percent differences between reported dose and true dose delivered are < 5% for the 1000–3000 cGy using equations 9 and 11.

Table 4: Summary of calculated dose and percent difference to the actual dose delivered.

Delivered Dose (cGy)	630–640 nm		670–680 nm	
	Calculated Dose (cGy)	% Difference	Calculated Dose (cGy)	% Difference
100	100.8	0.8	81.9	18.1
500	504.3	0.9	566.8	13.4
1000	863.0	13.7	1031.0	3.1
2000	`1281.7	35.9	2075.5	3.8
3000	1505.2	49.8	2872.0	4.3

These results show that a radiochromic dosimeter using both crystal forms of LiPCDA (635LiPCDA and 674LiPCDA) can measure dose as low as 100 cGy with <1 % difference, and probably lower[40], although not confirmed in these sets of experiments. However, the spectral window needs to be shifted to 670-680 nm to measure doses >500cGy with a <5% difference. For doses >3000 cGy this algorithm for calculated dose, regardless of which wavelength window is used, may not be valid. This is because the percent difference between delivered and calculated dose demonstrated an increasing trend with dose. To ensure that the dynamic range of the combined measurements can be extended, further testing is needed.

2.4 Conclusions on modified EBT-3

The 674LiPCDA produced through desiccation of commercial EBT-3 film was observed to be structurally indistinguishable with SEM from the native form but turned out to be ~3x less sensitive to dose resulting in a higher dynamic range. Although 674LiPCDA did share λ_{max} with PCDA ~675 nm, it was not observed to produce a linear dose response over a similar range[28]. The 635LiPCDA, which is specified to be sensitive between 10–2000 cGy as reported by its specifications[79], caused the radiochromic optical sensor to reach saturation ΔOD >2.5 when 3000 cGy was delivered. In contrast, the 674LiPCDA film produced a detectable signal response up to 7000 cGy while being below the saturation limits of the optical system and above detection limits of the transmitted photons. Despite having a lower sensitivity and larger dose sensitive range 674LiPCDA crystals showed no statistical difference in post-exposure kinetics when compared to 635LiPCDA at 1 h. However, at time intervals <1 h 635LiPCDA had higher percent increase in OD relative to 674LiPCDA, requiring further testing over a longer time range in order to validate difference in relative reaction rates. These differences in dosimetric behaviour between 635LiPCDA and 674LiPCDA are suggested to be caused by altering the crystal structure.

Specifically, the desiccation altered the packing structure of the monomers by removing enough water molecules to change the separation distance between monomers, resulting in a different dose response. This shows that the dosimetric behaviour of radiochromic crystals, which is dependant on structure, can be altered through use of small molecules that appear to cocrystalize with the monomers.

Chapter 3: Conclusion and future directions

3.1 Conclusions

In this thesis it was hypothesized that the dosimetric behaviour of radiochromic crystals is primarily dependent on structure, which may be a function of more than just the chemical composition of individual monomers. Specifically, without changing the chemistry of the monomers of LiPCDA the dose response may still be altered through a difference in packing structure and monomer separation through use of small molecules, such as water. In this research the dosimetric behaviour of the two dose sensitive forms of LiPCDA (635LiPCDA and 674LiPCDA produced by desiccating 635LiPCDA) were compared. It was found that 674LiPCDA was comparatively lower in dose sensitivity and had different polymerization kinetics and an extended dynamic range, suggesting that removal of water had actually altered the packing and suggesting that water forms a cocrystal with the radiochromic monomers. 674LiCPDA was shown to be a viable radiochromic dosimeter for potential use in real time *in vivo* dosimetry. It was also demonstrated that a dose measurement can be performed using both 635LiPCDA and 674LiPCDA simultaneously within a single fiber-optic path. While the combined sample showed dose sensitivity similar to 635LiPCDA at doses <500 cGy, an increasing trend in % difference between the calculated and the delivered dose was observed, and further testing is needed to report dose >3000 cGy. A combined film consisting of both 635LiPCDA and 674LiCPDA can be used as the dose sensitive component of a fiber optic probe dosimeter, taking advantage of both crystal forms.

3.2 Future Directions: Dose rate characterizations of 674LiPCDA

For applications in real-time *in vivo* dosimetry, any uncertainties in the real time dose measurement of the 674LiPCDA need to be characterized. One of these uncertainties is due to variable darkening of the film as a function of continuous dose deposition. This is because during exposure, the polymer resulting in the ΔOD at the wavelength of interest (around λ_{max}) takes some

finite time to form. At higher dose rates, this lag in polymer formation causes a lower ΔOD than expected. The post-exposure ΔOD of radiochromic film is a surrogate for the delay in polymer completion that occurs during exposure, and has been shown to be related to the dose rate[28,32]. The ΔOD of 635LiPCDA has been shown by Rink *et al.*[40] to have a percent standard deviation < 4.5% in ΔOD measurements from 16–520 cGy/min. Thus, a future hypothesis to test would be, 674LiPCDA has a dose rate dependence similar to 635LiPCDA and its rate of ΔOD increase is not proportional to the dose rate.

3.3 Future directions: Varying Li^+ molar ratio in LiPCDA to produce crystal mixtures

It was demonstrated in this thesis that a fiberized dosimeter configuration produced by combing the two radiochromic films 635LiPCDA and 674LiPCDA could potentially allow for an increased dynamic range while maintaining dose sensitivity down to 5 cGy as previously shown for EBT films[40]. This was done by simply stacking two films. Another potential way of using both 635LiPCDA and 674LiPCDA is to grow both crystals simultaneously in solution, and make coatings using the mixture for use as a dosimeter. This can be achieved by varying the molar ratio Li^+ to PCDA, where crystals that appear to have both the Li^+ and H^+ bonded monomers would have peak absorbance at 635 nm and crystals that have mostly Li^+ bonded monomers would have peak absorbance at 674 nm. Thus, it is expected that by increasing the Li^+ concentration the dominant crystal form can be shifted from 635LiPCDA to 674LiPCDA and at some molar ratio of Li^+: PCDA both crystal forms will be present. Preliminary investigations support this hypothesis and have demonstrated that radiochromic crystals with both absorbance peaks (~635 nm and ~674 nm) can be obtained at 0.6:1 stoichiometric ratio of Li^+ to PCDA. Figure 15 shows the absorbance spectra of solutions with varying stoichiometric ratios of Li^+: PCDA from 0.2:1 to 1:1. As the Li^+ ratio

increases, the 635 nm peak maximum shrinks in intensity, while the 674 nm peak grows. Figure 16 shows the resultant SEM image of the 0.6:1 Li^+ to PCDA crystal structure at 3500x magnification with both "plate-like" and "hair-like" crystals present.

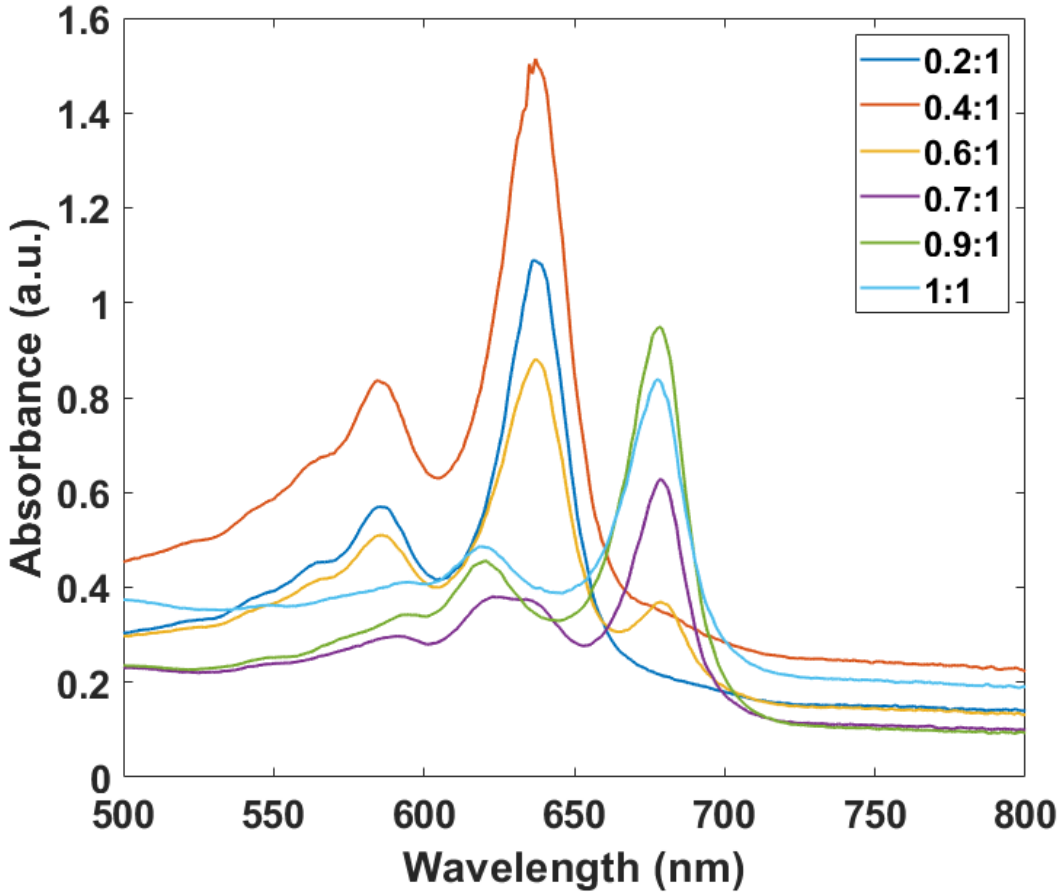

Figure 15: Varying molar ratio of Li^+ to PCDA solutions, exposed with UV light to produce absorbance spectra. No thickness correction was applied.

The data shows that not only are both absorbance peaks present at this ratio, but both macroscopic crystal structures are also present. By further investigating absorbance peaks of the Li^+ concentration series between molar ratios ranging from 0.6:1 to 0.9:1 an optimal molar ratio can be determined. An ideal mixture of crystals would have a sufficient absorbance signal from both characteristic absorbance peaks to measure dose. A radiochromic dosimeter using this

optimized mixture would have low dose sensitivity due to the 635LiPCDA and the dynamic range of the 674LiPCDA.

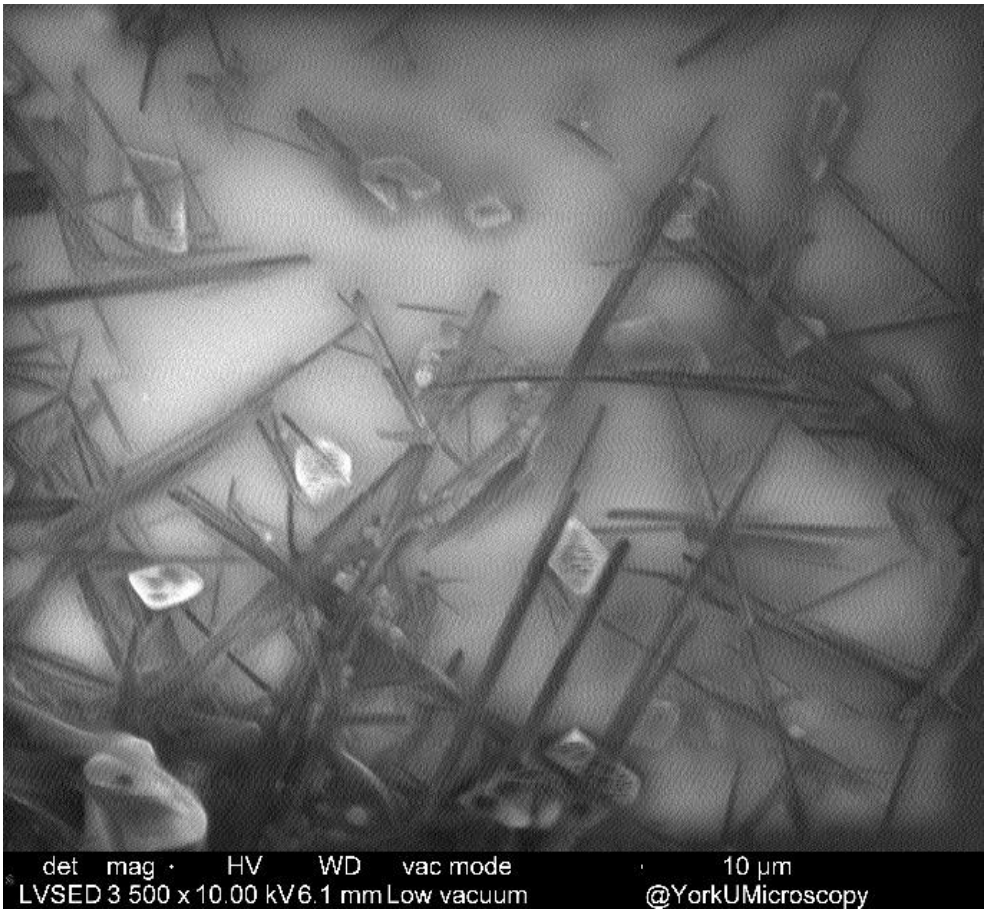

Figure 16: SEM image of a 0.6:1 ratio of Li^+ to PCDA mixture which had absorbance peaks at 635 nm and 674 nm. Image was taken at 3500x magnification.

3.4 Future directions: A two-point verification of dose from spatially separated films

Secondary simultaneous verification of dose from a different location of the same optical fiber dosimeter increases the measurement's confidence and provides extra information about the dose distribution. This is not possible when using just one form of LiPCDA as multiple films of the same form would not provide any unique information. When two forms of LiPCDA (635LiPCDA and 674LiPCDA) are measured simultaneously, both spectral peaks are observed,

occurring at the expected ~635 nm and ~674 nm wavelengths. These two peaks are ~40 nm apart, sufficiently spaced to allow for a 10 nm integration window around each peak to determine the ΔOD_{net} signal for each film. In the configuration described in this thesis, the radiochromic dosimeter is able to measure dose from a single point in space. Therefore, by measuring the true dose delivered at multiple points during a treatment the confidence of the measured dose increases. With multiple spatially separated film formats such as 635LiPCDA and 674LiPCDA it is possible to measure the dose at two points of interest in real time through a single dosimeter. The dose would then be determined by solving the system of equations 12–16, where D_1 and D_2 is the dose absorbed by DesEBT-3 and EBT-3, respectively.

$$\Delta OD^{\lambda_n-\lambda_1}_{measured\ total} = \Delta OD^{\lambda_n-\lambda_1}_{EBT3} + \Delta OD^{\lambda_n-\lambda_1}_{DesEBT3} \quad (12)$$

$$\Delta OD^{630-640}_{DesEBT3} = p_1(D_1)^3 + p_2(D_1)^2 + p_3(D_1) + p_4 \quad (13)$$

$$\Delta OD^{630-640}_{EBT3} = p_5(D_2)^3 + p_6(D_2)^2 + p_7(D_2) + p_8 \quad (14)$$

$$\Delta OD^{670-680}_{DesEBT3} = p_9(D_1)^3 + p_{10}(D_1)^2 + p_{11}(D_1) + p_{12} \quad (15)$$

$$\Delta OD^{670-680}_{EBT3} = p_{13}(D_2)^3 + p_{14}(D_2)^2 + p_{15}(D_2) + p_{16} \quad (16)$$

Unlike in the example used in Section 2.3.5, in this configuration the dose absorbed by each film would not be the same. The absorbance spectra from the spatially separated films are expected to be similar to Figure 14, as this would also be the combined absorbance of 635LiPCDA and 674LiPCDA. The polynomial fitting coefficients p_1 –p_{16} are determined by fitting in a similar process described in section 2.2.5 To validate this method of measuring dose distributions in real time an apparatus to hold two film holders was designed and prototyped to fit within the existing phantom. Future work will look to design and build a phantom that can accommodate two film holders and collect the combined absorbance spectra from spatially separated films and compare

delivered dose to reported dose. For dose distribution measurements the films would be placed in their own individual film holders with interrogation light travelling through each film before detection at the spectrophotometer. A schematic representation of this configuration is shown in Figure 17.

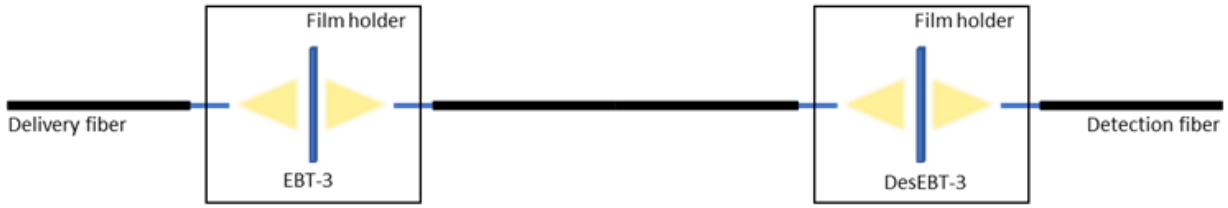

Figure 17 Schematic diagram of a spatially separated film measurement.

3.5 Future directions: Integrating an IR calibration dye into a fiber optic probe dosimeter

In recent years commercial Gafchromic® films have been used for real-time readout of dose[80,81]. To meet the recommendation set by IEAE for *in vivo* dosimetry, a fiber optic probe dosimeter based on radiochromic materials was designed and fabricated by Rink *et al.*[82,83]. One of the challenges of fabricating a miniature dosimeter with micron-thick coating is the reproducibility and uncertainty in the coating itself. For a given radiochromic formulation, film sensitivity is dependent on the monomer packing and the coating thickness. Future work will focus on optically calibrating for the thickness of radiochromic material, and thus accounting for sensitivity of any individual probe. In our approach, calibration will be performed through a homogeneously incorporated infra-red (IR) dye in the radiochromic film. A homogeneously dispersed IR dye can be used to measure the thickness of the film given a priori knowledge of the concentration, extinction coefficient, and peak absorbance of the dye, according to the Beer-Lambert law ($A = \varepsilon cl$). The path length (l) of the interrogation light through the film is equated to

the amount of radiochromic material for a given formulation. An IR dye is needed in order to avoid interference (spectral overlap) with the absorbance spectrum of the radiochromic material. Also since optical fibers are poor transmitters of UV/blue light, IR wavelengths are better suited as the calibration dye for optimal fiber optic signal transmission. Furthermore, fibers that transmit in the IR are also more ubiquitous and cheaper than alternatives, such as those in the UV. Figure 18 shows a schematic diagram of a previously developed fiber optic probe dosimeter with an IR dye incorporated into the coating and preliminary absorbance spectra collected upon UV exposure. Our previously designed and developed probe prototypes utilized plastic optical fibers, a thin film of LiPCDA and a dielectric mirror for transmission-reflection spectroscopy as shown in Figure 18. In this reflection mode configuration, the interrogation light would travel through the radiochromic film twice before reaching the detector. Preliminary coatings of 635LiPCDA and IR-783 dye were made. Both absorbance peaks from the radiochromic material and IR dye (the latter shifted from 783 nm to 800 nm in radiochromic suspension) were observed using a Cary 500 spectrophotometer. The absorbance peak of IR-783 was stable with increased UV exposure as shown by Figure 18, confirming that is does not degrade with UV radiation exposure. Since the IR-783 dye absorbance peak is stable with radiation exposure, only a simple background subtraction of the IR dye absorbance in the 630-640 nm band is needed to measure the change in absorbance from the radiochromic material. Future work will determine the optimal concentration of IR dye needed to produce an absorbance signal of ~0.5, needed for sufficient signal to noise ratio to measure submicron film thickness. Next, calibration curves of absorbance against thickness will be produced and used to characterize the dose response of the combined formulation. These future steps will allow for thickness dependent sensitivity calibration of the radiochromic fiber optic probe dosimeter.

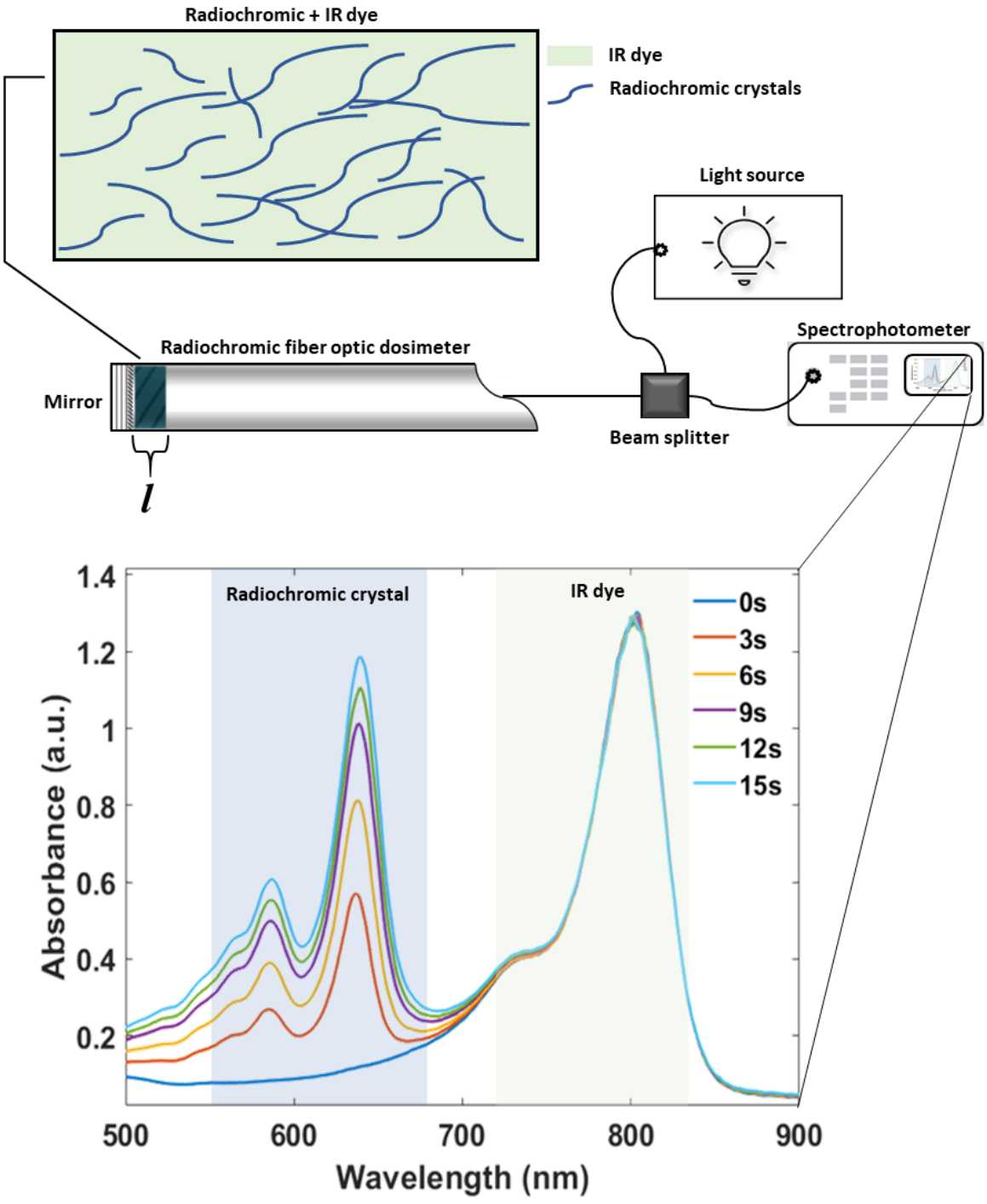

Figure 18: Schematic of optical dosimeter probe construction with dye-integrated radiochromic film[84] With preliminary data showing change in absorbance of LiPCDA coatings on Mylar™ substrate with IR-783 integrated as a function of time irradiated with 254 nm UV light.

3.6 Summary

In this thesis the dosimetric behaviour of desiccated 635LiPCDA (674LiPCDA) was investigated and compared to 635LiPCDA. It was found that 674LiPCDA had ~3x lower dose sensitivity, a dynamic range up to 7000 cGy and faster post-exposure kinetics relative to 635LiPCDA. 674LiPCDA was also non-linear in dose response similar to 635LiPCDA. These findings support the hypothesis that the monomer packing of radiochromic crystals and dosimetric behaviour is more than just a function of their chemical composition, modifiable through use of small molecules, such as water, incorporated into the crystal structure. In terms of clinical applications, 674LiCPDA can be used in combination with 635LiCPDA to produce an *in vivo* real-time dosimeter with simultaneously high dose sensitivity and high dynamic range. Future work will continue to develop combined films and integrate an IR dye into the radiochromic probe dosimeter developed by Rink *et al.*[82,83]. The integration of the IR-dye will fulfill the requirement for sensitivity calibration measurements done by to measuring the amount of radiochromic material before a treatment. While this work showed an important understanding, that the dosimetric behaviour of the radiochromic film can be manipulated without changing the monomer chemistry, future work remains to be done as described here. Translational studies are also currently underway towards the development of an optimal radiochromic probe dosimeter technology.

References

1. Brenner DR, Weir HK, Demers AA, et al. Projected estimates of cancer in Canada in 2020. *Can Med Assoc J*. 2020;192(9):E199-E205. doi:10.1503/cmaj.191292

2. Baskar R, Lee KA, Yeo R, Yeoh K-W. Cancer and Radiation Therapy: Current Advances and Future Directions. *Int J Med Sci*. 2012;9(3):193-199. doi:10.7150/ijms.3635

3. Radiation Therapy for Cancer - National Cancer Institute. Published April 29, 2015. Accessed March 6, 2021. https://www.cancer.gov/about-cancer/treatment/types/radiation-therapy

4. Baskar R, Dai J, Wenlong N, Yeo R, Yeoh K-W. Biological response of cancer cells to radiation treatment. *Front Mol Biosci*. 2014;1:24. doi:10.3389/fmolb.2014.00024

5. Hubenak JR, Zhang Q, Branch CD, Kronowitz SJ. Mechanisms of Injury to Normal Tissue after Radiotherapy: A Review. *Plast Reconstr Surg*. 2014;133(1):49e-56e. doi:10.1097/01.prs.0000440818.23647.0b

6. Barnett GC, West CML, Dunning AM, et al. Normal tissue reactions to radiotherapy: towards tailoring treatment dose by genotype. *Nat Rev Cancer*. 2009;9(2):134-142. doi:10.1038/nrc2587

7. Roach MC, Bradley JD, Robinson CG. Optimizing radiation dose and fractionation for the definitive treatment of locally advanced non-small cell lung cancer. *J Thorac Dis*. 2018;10(S21):S2465-S2473. doi:10.21037/jtd.2018.01.153

8. Safety Commission CN. Radiation doses. Published February 3, 2014. Accessed April 19, 2021. http://nuclearsafety.gc.ca/eng/resources/radiation/introduction-to-radiation/radiation-doses.cfm

9. Klein EE, Hanley J, Bayouth J, et al. Task Group 142 report: Quality assurance of medical acceleratorsa): Task Group 142 Report: QA of Medical Accelerators. *Med Phys*. 2009;36(9Part1):4197-4212. doi:10.1118/1.3190392

10. Quality assurance guidelines for radiation treatment – CPAC. Canadian Partnership Against Cancer. Accessed March 6, 2021. https://www.partnershipagainstcancer.ca/topics/quality-assurance-guidelines-radiation-treatment/

11. Kutcher GJ, Coia L, Gillin M, et al. *Comprehensive QA for Radiation Oncology*. AAPM; 1994. doi:10.37206/45

12. Baek TS, Chung EJ, Son J, Yoon M. Feasibility Study of Patient Specific Quality Assurance Using Transit Dosimetry Based on Measurement with an Electronic Portal Imaging Device. *Prog Med Phys*. 2017;28(2):54. doi:10.14316/pmp.2017.28.2.54

13. McDermott LN, Wendling M, Sonke J-J, van Herk M, Mijnheer BJ. Replacing Pretreatment Verification With In Vivo EPID Dosimetry for Prostate IMRT. *Int J Radiat Oncol*. 2007;67(5):1568-1577. doi:10.1016/j.ijrobp.2006.11.047

14. Otto K. Volumetric modulated arc therapy: IMRT in a single gantry arc: Single arc radiation therapy. *Med Phys*. 2007;35(1):310-317. doi:10.1118/1.2818738

15. Palma DA, Verbakel WFAR, Otto K, Senan S. New developments in arc radiation therapy: A review. *Cancer Treat Rev*. 2010;36(5):393-399. doi:10.1016/j.ctrv.2010.01.004

16. Cheung K. Intensity modulated radiotherapy: advantages, limitations and future development. *Biomed Imaging Interv J*. 2006;2(1). doi:10.2349/biij.2.1.e19

17. Guckenberger M, Meyer J, Wilbert J, et al. Cone-beam CT based image-guidance for extracranial stereotactic radiotherapy of intrapulmonary tumors. *Acta Oncol*. 2006;45(7):897-906. doi:10.1080/02841860600904839

18. Teoh M, Clark CH, Wood K, Whitaker S, Nisbet A. Volumetric modulated arc therapy: a review of current literature and clinical use in practice. *Br J Radiol*. 2011;84(1007):967-996. doi:10.1259/bjr/22373346

19. Li Y, Wang J, Tan L, et al. Dosimetric comparison between IMRT and VMAT in irradiation for peripheral and central lung cancer. *Oncol Lett*. Published online January 4, 2018. doi:10.3892/ol.2018.7732

20. Vanneste BGL, Van Limbergen EJ, van Lin EN, van Roermund JGH, Lambin P. Prostate Cancer Radiation Therapy: What Do Clinicians Have to Know? *BioMed Res Int*. 2016;2016:1-14. doi:10.1155/2016/6829875

21. Kamperis E, Kodona C, Hatziioannou K, Giannouzakos V. Complexity in Radiation Therapy: It's Complicated. *Int J Radiat Oncol*. 2020;106(1):182-184. doi:10.1016/j.ijrobp.2019.09.003

22. *Development of Procedures for In Vivo Dosimetry in Radiotherapy*. INTERNATIONAL ATOMIC ENERGY AGENCY; 2013. https://www.iaea.org/publications/8962/development-of-procedures-for-in-vivo-dosimetry-in-radiotherapy

23. Mijnheer B, Beddar S, Izewska J, Reft C. In vivo dosimetry in external beam radiotherapy: *Med Phys*. 2013;40(7):070903. doi:10.1118/1.4811216

24. Peca S, Sinha RS, Brown DW, Smith WL. *In vivo* Portal Imaging Dosimetry Identifies Delivery Errors in Rectal Cancer Radiotherapy on the Belly Board Device. *Technol Cancer Res Treat*. 2017;16(6):956-963. doi:10.1177/1533034617711519

25. Ortiz López P, Cosset JM, Dunscombe P, et al. ICRP publication 112. A report of preventing accidental exposures from new external beam radiation therapy technologies. *Ann ICRP*. 2009;39(4):1-86. doi:10.1016/j.icrp.2010.02.002

26. Essers M, Mijnheer B. In vivo dosimetry during external photon beam radiotherapy. *Int J Radiat Oncol*. 1999;43(2):245-259. doi:10.1016/S0360-3016(98)00341-1

27. Rink A. Point-based ionizing radiation dosimetry using radiochromic materials and a fibreoptic readout system. Published online June 2008. https://tspace.library.utoronto.ca/handle/1807/11254?mode=full

28. Rink A, Vitkin IA, Jaffray DA. Suitability of radiochromic medium for real-time optical measurements of ionizing radiation dose: Radiochromic medium in real-time measurements of radiation dose. *Med Phys*. 2005;32(4):1140-1155. doi:10.1118/1.1877832

29. Marroquin EYL, Herrera González JA, Camacho López MA, Barajas JEV, García-Garduño OA. Evaluation of the uncertainty in an EBT3 film dosimetry system utilizing net optical density. *J Appl Clin Med Phys*. 2016;17(5):466-481. doi:10.1120/jacmp.v17i5.6262

30. Lavallée M-C, Gingras L, Beaulieu L. Energy and integrated dose dependence of MOSFET dosimeter sensitivity for irradiation energies between 30kV and Co60: Energy and integrated dose dependence of MOSFET sensitivity. *Med Phys*. 2006;33(10):3683-3689. doi:10.1118/1.2349301

31. Podgorsak EB. *Radiation Oncology Physics: A Handbook for Teachers and Students*. International Atomic Energy Agency; 2005.

32. Rink A, Vitkin IA, Jaffray DA. Characterization and real-time optical measurements of the ionizing radiation dose response for a new radiochromic medium: Real-time optical measurements of new radiochromic medium. *Med Phys*. 2005;32(8):2510-2516. doi:10.1118/1.1951447

33. Dutreix A, Bridier A. *Dosimetry for External Beams of Photon and Electron Radiation*. Academic Press Inc; 1985. http://inis.iaea.org/search/search.aspx?orig_q=RN:19018105

34. Devic S. Radiochromic film dosimetry: Past, present, and future. *Phys Med*. 2011;27(3):122-134. doi:10.1016/j.ejmp.2010.10.001

35. Niroomand-Rad A, Blackwell CR, Coursey BM, et al. Radiochromic film dosimetry: Recommendations of AAPM Radiation Therapy Committee Task Group 55. *Med Phys*. 1998;25(11):2093-2115. doi:10.1118/1.598407

36. Williams M, Metcalfe P, Rosenfeld A, Kron T, d'Errico F, Moscovitch M. Radiochromic Film Dosimetry and its Applications in Radiotherapy. In: ; 2011:75-99. doi:10.1063/1.3576160

37. Yao T, Luthjens LH, Gasparini A, Warman JM. A study of four radiochromic films currently used for (2D) radiation dosimetry. *Radiat Phys Chem*. 2017;133:37-44. doi:10.1016/j.radphyschem.2016.12.006

38. Todorovic M, Fischer M, Cremers F, Thom E, Schmidt R. Evaluation of GafChromic EBT prototype B for external beam dose verification: Evaluation of EBT film for external beam verification. *Med Phys*. 2006;33(5):1321-1328. doi:10.1118/1.2188077

39. Akbas U, Kesen ND, Koksal C, Okutan M, Demir B, Becerir HB. Surface dose measurement with Gafchromic EBT3 film for intensity modulated radiotherapy technique. Aydin A, Sarpün IH, Tel E, Kaplan A, Demir B, eds. *EPJ Web Conf*. 2017;154:01011. doi:10.1051/epjconf/201715401011

40. Rink A, Vitkin IA, Jaffray DA. Intra-irradiation changes in the signal of polymer-based dosimeter (GAFCHROMIC EBT) due to dose rate variations. *Phys Med Biol*. 2007;52(22):N523-N529. doi:10.1088/0031-9155/52/22/N03

41. Niroomand-Rad A, Chiu-Tsao S, Grams MP, et al. Report of AAPM Task Group 235 Radiochromic Film Dosimetry: An Update to TG-55. *Med Phys*. 2020;47(12):5986-6025. doi:10.1002/mp.14497

42. Bissler H. Photopolymerization of Diacetylenes. In: ; 2005.

43. Okuno T, Izuoka A, Kume K, Sato N, Sugawara T. Crystal Structure and Solid State Reactivity of Unsymmetrically Aryl-Substituted Diacetylene. *Mol Cryst Liq Cryst Sci Technol Sect Mol Cryst Liq Cryst*. 1993;225(1):393-398. doi:10.1080/10587259308036244

44. Zachmann HG. Polydiacetylenes. In: *Advances in Polymer Science/Fortschritte Der Hochpolymeren-Forschung*. Vol 79. ; 1984. Accessed February 5, 2021. http://www.degruyter.com/doi/10.1524/zpch.1972.79.1_2.112

45. Beddar S, Beaulieu L, eds. *Scintillation Dosimetry*. CRC Press; 2016. doi:10.1201/b19491

46. Nakanishi H, Jones W, Thomas JM, Hasegawa M, Rees WL. Topochemically Controlled Solid-State Polymerization. *Proc R Soc Lond Ser Math Phys Sci*. 1980;369(1738):307-325.

47. Lauher JW, Fowler FW, Goroff NS. Single-Crystal-to-Single-Crystal Topochemical Polymerizations by Design. *Acc Chem Res*. 2008;41(9):1215-1229. doi:10.1021/ar8001427

48. Baughman RH. Solid-state synthesis of large polymer single crystals. *J Polym Sci Polym Phys Ed*. 1974;12(8):1511-1535. doi:10.1002/pol.1974.180120801

49. Baughman RH, Yee KC. Solid-state polymerization of linear and cyclic acetylenes. *J Polym Sci Macromol Rev*. 1978;13(1):219-239. doi:10.1002/pol.1978.230130104

50. Chance RR, Baughman RH, Müller H, Eckhardt CJ. Thermochromism in a polydiacetylene crystal. *J Chem Phys*. 1977;67(8):3616-3618. doi:10.1063/1.435361

51. Baughman RH. Solid-state polymerization of diacetylenes. *J Appl Phys*. 1972;43(11):4362-4370. doi:10.1063/1.1660929

52. Li Z, Fowler FW, Lauher JW. Weak Interactions Dominating the Supramolecular Self-Assembly in a Salt: A Designed Single-Crystal-to-Single-Crystal Topochemical Polymerization of a Terminal Aryldiacetylene. *J Am Chem Soc*. 2009;131(2):634-643. doi:10.1021/ja806663h

53. Grim PCM, De Feyter S, Gesquière A, et al. Submolecularly Resolved Polymerization of Diacetylene Molecules on the Graphite Surface Observed with Scanning Tunneling Microscopy. *Angew Chem Int Ed Engl*. 1997;36(23):2601-2603. doi:10.1002/anie.199726011

54. Rink A, Lewis DF, Varma S, Vitkin IA, Jaffray DA. Temperature and hydration effects on absorbance spectra and radiation sensitivity of a radiochromic medium: Temperature and hydration effects on radiochromic medium. *Med Phys*. 2008;35(10):4545-4555. doi:10.1118/1.2975483

55. Guillet J. *Polymer Photophysics and Photochemistry: An Introduction to the Study of Photoprocesses in Macromolecules*. Cambridge University Press,New York, NY; 1987. https://www.osti.gov/biblio/6748297

56. McLaughlin WL, Yun-Dong C, Soares CG, Miller A, Van Dyk G, Lewis DF. Sensitometry of the response of a new radiochromic film dosimeter to gamma radiation and electron beams. *Nucl Instrum Methods Phys Res Sect Accel Spectrometers Detect Assoc Equip*. 1991;302(1):165-176. doi:10.1016/0168-9002(91)90506-L

57. Saylor MC, Tamargo TT, McLaughlin WL, Khan HM, Lewis DF, Schenfele RD. A thin film recording medium for use in food irradiation. *Spec Issue Prog Radiat Process*. 1988;31(4):529-536. doi:10.1016/1359-0197(88)90222-6

58. Kim MO, Lee JS. The effect of 10,12-pentacosadiynoic acid on the morphology and characteristics of electrospun PDA/PU nanofibers. *Fash Text*. 2019;6(1):27. doi:10.1186/s40691-019-0183-3

59. Patel GN, Miller GG. Structure-property relationships of diacetylenes and their polymers. *J Macromol Sci Part B*. 1981;20(1):111-131. doi:10.1080/00222348108219431

60. Ali I, Costescu C, Vicic M, Dempsey JF, Williamson JF. Dependence of radiochromic film optical density post-exposure kinetics on dose and dose fractionation. *Med Phys*. 2003;30(8):1958-1967. doi:10.1118/1.1587611

61. Cheung T, Butson MJ, Yu PKN. Post-irradiation colouration of Gafchromic EBT radiochromic film. *Phys Med Biol*. 2005;50(20):N281-N285. doi:10.1088/0031-9155/50/20/N04

62. Kalef-Ezra J, Karava K. Radiochromic film dosimetry: Reflection vs transmission scanning. *Med Phys*. 2008;35(6Part1):2308-2311. doi:https://doi.org/10.1118/1.2919092

63. Klassen NV, van der Zwan L, Cygler J. GafChromic MD-55: Investigated as a precision dosimeter. *Med Phys*. 1997;24(12):1924-1934. doi:10.1118/1.598106

64. van Battum LJ, Hoffmans D, Piersma H, Heukelom S. Accurate dosimetry with GafChromic^{TM} EBT film of a 6MV photon beam in water: What level is achievable?: Accurate dosimetry with GafChromic^{TM} EBT film in water. *Med Phys*. 2008;35(2):704-716. doi:10.1118/1.2828196

65. Butson MJ, Cheung T, Yu PKN. Scanning orientation effects on Gafchromic EBT film dosimetry. *Australas Phys Eng Sci Med*. 2006;29(3):281-284. doi:10.1007/BF03178579

66. Vaiano P, Consales M, Casolaro P, et al. A novel method for EBT3 Gafchromic films read-out at high dose levels. *Phys Med*. 2019;61:77-84. doi:10.1016/j.ejmp.2019.04.013

67. Seto K, Hosoi Y, Furukawa Y. Raman spectra of Langmuir–Blodgett and Langmuir–Schaefer films of polydiacetylene prepared from 10,12-pentacosadiynoic acid. *Chem Phys Lett*. 2007;444(4-6):328-332. doi:10.1016/j.cplett.2007.07.043

68. Talarico OS, Krylova TA, Melnik NN. Raman scattering for dosimetry using GAFCHROMIC EBT 3 radiochromic dosimetry film. *Med Phys*. 2019;46(4):1883-1887. doi:10.1002/mp.13423

69. Enkelmann V. Structural aspects of the topochemical polymerization of diacetylenes. In: Cantow H-J, ed. *Polydiacetylenes*. Vol 63. Advances in Polymer Science. Springer Berlin Heidelberg; 1984:91-136. doi:10.1007/BFb0017652

70. Shufang Y, Huilin Z, Pingsheng H. X-ray diffraction analysis of 10,12-pentacosadiynoic acid Langmuir-Blodgett films during polymerization. Published online 1999:6.

71. Hall AV, Yufit DS, Apperley DC, et al. The crystal engineering of radiation-sensitive diacetylene cocrystals and salts. *Chem Sci*. 2020;11(30):8025-8035. doi:10.1039/D0SC02540B

72. Patel GN, Chance RR, Witt JD. A planar–nonplanar conformational transition in conjugated polymer solutions. *J Chem Phys*. 1979;70(9):4387-4392. doi:10.1063/1.438012

73. Garchromic EBT Films - GAFchromic^{TM}. Accessed February 5, 2021. http://www.gafchromic.com/gafchromic-film/radiotherapy-films/EBT/index.asp

74. Rink A, Vitkin IA, Jaffray DA. Energy dependence (75kVp to 18MV) of radiochromic films assessed using a real-time optical dosimeter: Energy dependence of radiochromic films in real-time measurements. *Med Phys*. 2007;34(2):458-463. doi:10.1118/1.2431425

75. Borca VC, Pasquino M, Russo G, et al. Dosimetric characterization and use of GAFCHROMIC EBT3 film for IMRT dose verification. *J Appl Clin Med Phys*. 2013;14(2):158-171. doi:10.1120/jacmp.v14i2.4111

76. Lewis D, Micke A, Yu X, Chan MF. An efficient protocol for radiochromic film dosimetry combining calibration and measurement in a single scan: Efficient protocol for radiochromic film dosimetry. *Med Phys*. 2012;39(10):6339-6350. doi:10.1118/1.4754797

77. HALL A. The Topochemical Polymerisation of Radiation-Sensitive 10,12-Pentacosadiynoic Acid as Different Multicomponent Solid Forms. Published online 2020. Accessed March 15, 2021. http://etheses.dur.ac.uk/13763/

78. Brown JM, Carlson DJ, Brenner DJ. The Tumor Radiobiology of SRS and SBRT: Are More Than the 5 Rs Involved? *Int J Radiat Oncol*. 2014;88(2):254-262. doi:10.1016/j.ijrobp.2013.07.022

79. GAFChromic Film, EBT3-1417, 13" x 17" (10/Box) - Radiation Products Design, Inc. Accessed March 22, 2021. https://www.rpdinc.com/gafchromic-film-ebt3-13-x-17-inch-246.html

80. Casolaro P, Campajola L, Breglio G, et al. Real-time dosimetry with radiochromic films. *Sci Rep*. 2019;9(1):5307. doi:10.1038/s41598-019-41705-0

81. Buontempo S, Campajola L, Casolaro P, Fienga F; Istituto Nazionale Di Fisica Nucleare. Method and system for real-time determination of characteristics of radio-chromic films. WO 2019/138309 A1 July 18, 2019.

82. Rink A, Jaffray D, Vitkin IA; University Health Network. Apparatus and method for determining radiation dose. US 7,399,977,B2. July 15, 2008.

83. Rink A, Jaffray D, Mermut O, Caron S, Croteau A, Roy-Moisan F; Institut National D'Optique, University Health Network. Fiber optic radiochromic dosimeter probe and method to make the same. US 9,000,401 B2. April 7, 2015.

84. Kaiyum R. Optical Calibration of Radiochromic Film Thickness With IR Dye. Poster presented at the: American Association of Physicists in Medicine and Canadian Organization of Medical Physicists Joint Annual Meeting; July 12, 2020; Virtual.

85. Knoll GF. *Radiation Detection and Measurement*. 4th ed. John Wiley; 2010.

86. Harris DC, Bertolucci MD. *Symmetry and Spectroscopy an Introduction to Vibrational and Electronic Spectroscopy*.; 2014.

87. Steiner UE. Fundamentals of Photophysics, Photochemistry, and Photobiology. In: *Photodynamic Therapy*. Springer Berlin Heidelberg; 2014:25-58.

88. Callens MB, Crijns W, Depuydt T, et al. Modeling the dose dependence of the vis-absorption spectrum of EBT3 GafChromic^{TM} films. *Med Phys*. 2017;44(6):2532-2543. doi:10.1002/mp.12246

Appendices

A: Fundamental interactions of ionizing radiation with matter

Photoelectric effect, incoherent Compton scattering, and pair/triplet production are the photon attenuation mechanisms relevant to radiotherapy. Each of these mechanisms may occur individually or as a combination, though each mechanism has a range of energy and atomic number combinations in which it is the dominant method of photon attenuation, as shown in Figure A.1. Film samples of EBT-3 used in this thesis were irradiated with a 6 MV beam and had $Z_{eff} = 7.26$[29], which is within the Compton dominant region. Thus, photoelectric and pair/triplet production are considered to be negligible to the photon attenuation within these film samples.

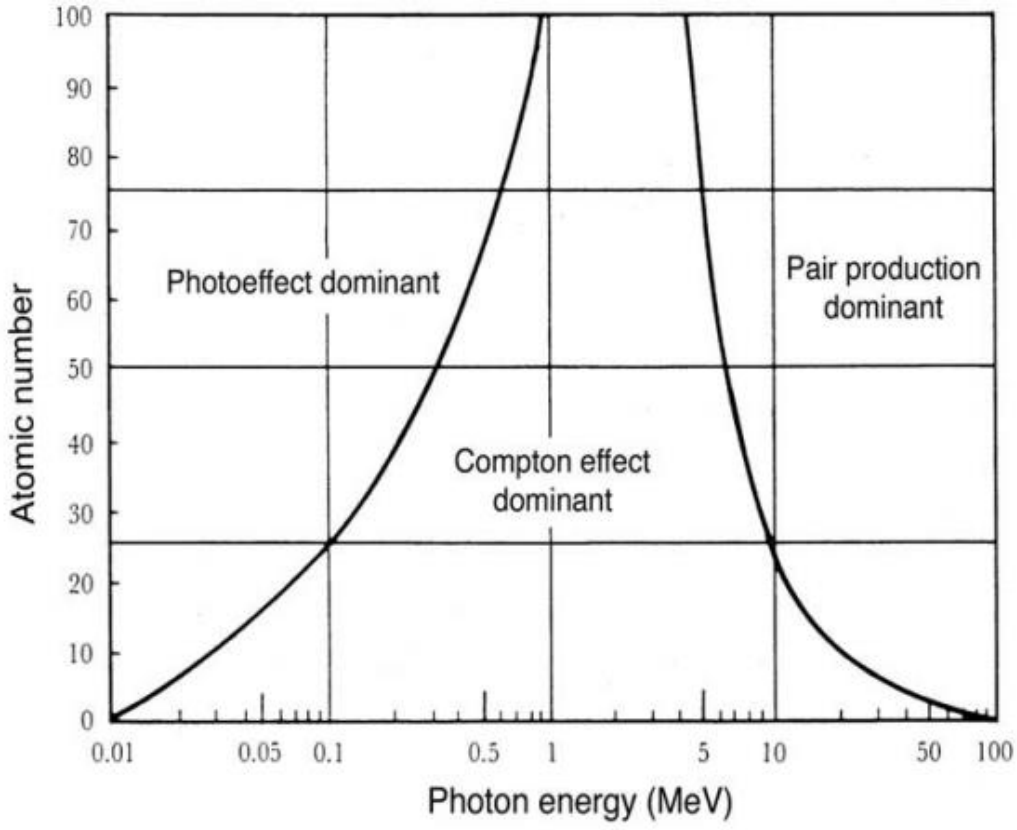

Figure A.1: Three main regions of high energy photon and matter interaction represented in terms of photon energy and atomic number of medium. Podgorsak[31]

In Compton scattering the incident photon interacts with an orbital or free electron imparting a portion of its energy to the electron as an inelastic collision, conserving energy, and momentum[85]. The photon is deflected through an angle θ with respect to its initial trajectory and has a lower energy as shown in Figure A.2. The electron known as a secondary electron, receives the difference in energy between the incident and scattered photon as kinetic energy and is ejected from the orbital. The secondary electron then deposits its energy into the surrounding matter along its trajectory through atomic excitations and ionizations as it slows down within the medium. Most of the dose is deposited into the medium by the secondary electrons.

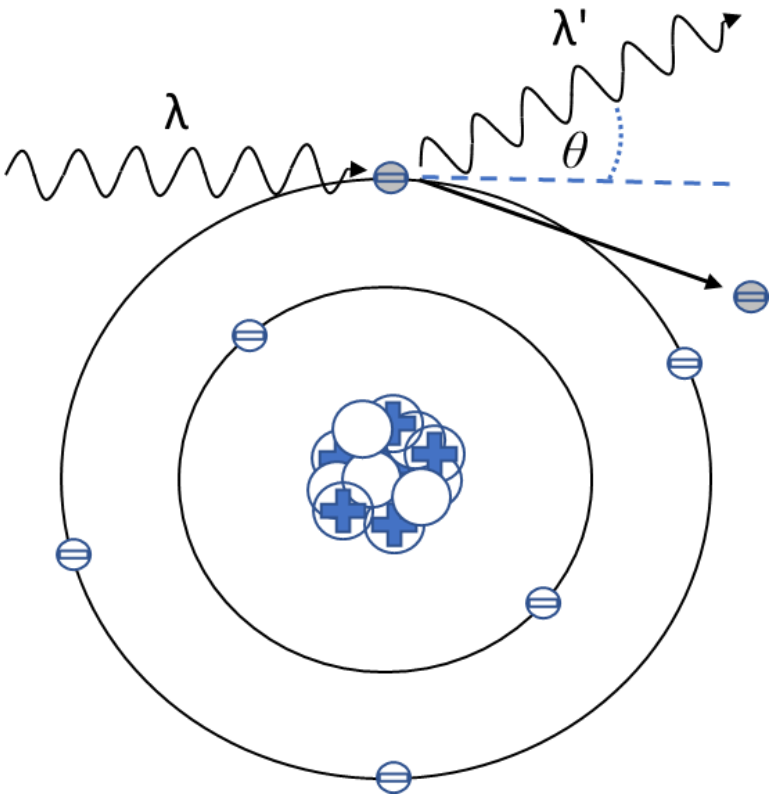

Figure A.2: Compton scattering occurring on a valence electron of a carbon atom. The scattered photon has shifted wavelength λ' and is deflected by an angle θ from the incident photon.

B: UV-Vis Spectroscopy

The absorption spectra observed in radiochromic materials such as LiPCDA are due to the overlapping π orbitals or conjugated π bonds of the carbon backbone. When a photon with sufficient energy interacts with the electrons in the highest occupied molecular orbital (HOMO) of these π bonds, the photon energy is absorbed by the electron[86]. The electron is then promoted to the lowest unoccupied molecular orbital (LUMO) of a higher energy state, π^*. This promotion is referred to as a π to π^* electronic transition[87]. The amount of energy needed to excite a π orbital electron is equivalent to the difference in energy (ΔE) between the HOMO and LUMO states. However, with increasing π conjugations, the ΔE between these states decreases. Then as lower-energy light is absorbed to promote electrons in systems with high π conjugated bonds, the peak absorbance λ_{max} increases following the relation $\Delta E = \frac{hc}{\lambda}$. An energy diagram representation of the HOMO-LUMO transition and ΔE with increasing conjugation is shown in Figure B.1. The peak absorbance of LiPCDA occurs at 635 nm indicating a high number of π bond conjugations; the overall spectra however is the average of many energy states and conjugation lengths.

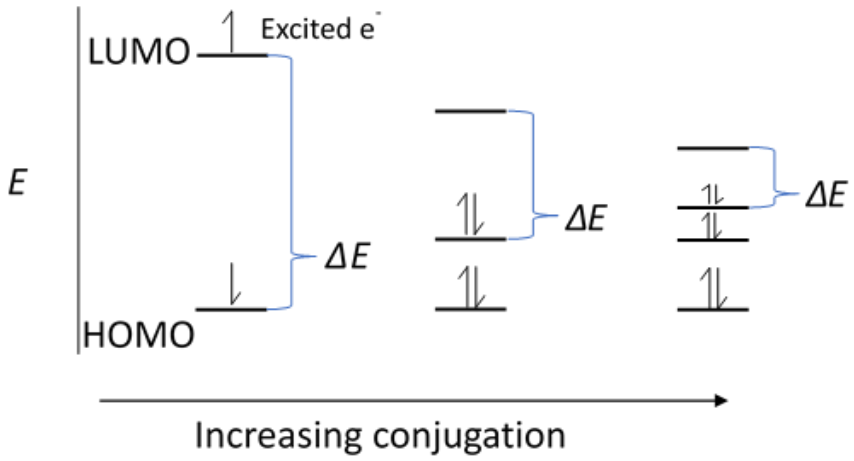

Figure B.1: Energy diagram of the HOMO-LUMO states and visual representation of the amount of energy absorbed with increasing π bond conjugations.

The dose-response of radiochromic film is measured as the change in absorbance (ΔA) at a particular wavelength, typically the λ_{max}. The ΔA in an ideal no-noise system is simply defined as the log ratio of the initial light intensity ($I(\lambda)_0$) against the transmitted light intensity ($I(\lambda)$) as shown by equation B.1. It is assumed that for radiochromic films, the only significant light attenuation is due to absorption, and attenuation from light scattering and reflection is negligible[88]. The ($I(\lambda)_0$) is equivalent to the transmitted light through a film sample before exposure, in this case a film sample is used as its own reference measurement and light loss through the system can be ignored.

$$\Delta A(\lambda) = log_{10}(\frac{I(\lambda)_0}{I(\lambda)}) \tag{B.1}$$

The change in optical density (ΔOD) is then defined as the definite integration of the average absorbance using an absorbance window 10 nm around λ_{max}, as shown in equation B.2.

$$\Delta OD \equiv \frac{1}{\lambda_n - \lambda_1} \sum_{i=1}^{n-1} \left(\frac{\Delta A_i + \Delta A_{i+1}}{2} \right) (\lambda_{i+1} - \lambda_i) \tag{B.2}$$

The dose is then defined as the ΔOD at the end of irradiation, marked by an abrupt change in the rate of ΔOD. Once the irradiation is turned off, no new polymer reactions are taking place and any continued increase in absorbance is purely due to the formation of polymers of appropriate length to contribute to absorbance around λ_{max} from earlier initiated polymerizations.

C: Film thickness measurement

The overall radiation sensitivity of radiochromic films is not only dependent on the particular monomer spacing as discussed in this thesis, but also on the amount of active material present in the film. A future direction described in this thesis (Ch 3.5) is to use micron thick radiochromic films integrated in an optical fiber as a dosimeter. The reproducibility of the films adds a source of uncertainty impacting the sensitivity of the radiochromic films. A simple way to account for small variations in film thickness is through the Beer-Lambert law, $A=\varepsilon cl$ (Equation C.1) with *a priori* knowledge of the concentration of absorber and its molar absorptivity along with measured absorbance.

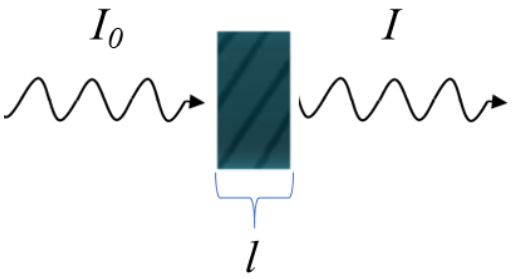

Figure C.1: Schematic diagram of light attenuation through a medium

$$A = log_{10}\left(\frac{I_0}{I}\right) = \varepsilon cl \qquad \text{(C.1)}$$

where I_0 is the initial light intensity, I is the transmitted light intensity, ε is the molar absorptivity, c is the molar concentration, and l is the path length.

It is assumed that the absorber is homogeneously integrated through the radiochromic coating (Figure C.1), and that the light attenuation of the absorber is primarily due to absorbance and the effects from scattering and reflection are negligible. Using this absorber, known ε and c of that absorber for the batch, and measured A for an individual probe, the pathlength of the radiochromic coating, and therefore sensitivity, can be calculated.

Page intentionally left blank